Master thesis

CARBON DOTS AS MARKERS FOR PLASTIC DEGRADATION ASSAYS

30^{th} of September, 2024

Nanobiotechnology, Yan Hess
Department of Materials and Production, Aalborg University

AALBORG UNIVERSITET
STUDENTERRAPPORT

Title:
Carbon dots as markers for plastic degradation assays

Theme:
Master thesis

Project period:
Fall 2023 - Spring 2024

Project participants:
Yan Hess

Supervisors:
Peter Fojan
Evamaria Petersen

Number of pages:
39

Finish date:
30^{th} of September, 2024

Aalborg University
Nanobiotechnology
Department of Materials and Production

Abstract:

This thesis focuses on the development of an assay using carbon dots (CD) as visual indicators of plastic degradation, specifically for screening proteins with catalytic activity towards polyethylene terephthalate (PET). CD were synthesised and integrated into PET substrates through spin-coating and electrospinning. PET fibers produced via electrospinning were found to be more suitable for the screening method, providing higher surface area and stability compared to PET films. Catalytic degradation assays were conducted using various proteins, where release of CD upon enzymatic degradation of the PET substrates was monitored using fluorescence emission spectroscopy and reversed-phase high-performance liquid chromatography. The results demonstrated that cutinase effectively degraded PET fibers, resulting in significant CD release inducing a visible fluorescent signal. However, the fluorescence response to substrate degradation by other proteins was less pronounced, indicating the need for further optimization. Despite the promising results with cutinase, inconsistencies in CD release as a direct indicator of PET degradation highlight the need for further refinement of the method.

Contents

List of Abbreviations

ACN	Acetonitrile
BHET	Bis(hydroxyethyl)terephthalate
CD	Carbon dots
DA	Deposition assay
DCM	Dichloromethane
DLS	Dynamic light scattering
DMF	Dimethylformamide
EG	Ethylene glycol
estDZ3mut	I144F M203Y mutant of Esterase DZ3, designed *in silico*.
estDZ3wt	wild-type of Esterase DZ3
FPLC	Fast protein liquid chromatography
HOMO	Highest Occupied Molecular Orbital.
IA	Immersion assay
IC	Internal Conversion.
IPTG	Isopropyl β-D-1-thiogalactopyranoside.
ISC	Intersystem Crossing.
LB	Lysogeny broth.
LUMO	Lowest Unocupied Molecular Orbital.
MHET	Mono(2-hydroxyethyl) terephthalate
PET	Polyethylene terephthalate
RP-HPLC	Reversed-phase high-performance liquid chromatography
SDS	Sodium dodecyl sulfate
SDS-PAGE	Sodium dodecyl sulfate polyacrylamide gel electrophoresis
TFA	Trifluoroacetic acid.
TPA	Terephtalic acid.
VR	Vibrational Relaxation.

1 Introduction

The impact of current large-scale production of synthetic polymers is of primary concern, as their negative-effects on soil health, human health and aquatic ecosystems continues to be increasingly documented [1, 2]. Aside from waste accumulation, recycling processes are limited in the recovery of component parts and are not environmentally friendly, leading to persistent pollution. Current recycling process are divided into primary, secondary and tertiary recycling, each with a different final product and limitations. Primary recycling reintegrates cleaner waste back into the production process, while secondary recycling use physical processes to transform post-consumer plastics into pellets or granules. Both methods are limited by the quality and contamination of the plastic waste that can be used. Tertiary recycling addresses these limitations by chemically degrading the synthetic polymers into smaller components, however, the process is energetically costly and leads to the release harmful chemicals into the environment [3, 4]. In contrast, biorecycling has the potential to overcome the limitations of both mechanical and chemical recycling by employing enzymes to reduce polymers into composing monomers, which can then be reused [5]. Although not yet fully scalable, the development of biorecycling has gained increasing attention with advances in biotechnology underscoring the viability of enzymatic degradation of polyethylene terephthalate (PET) [6], and it is starting to see commercial application [7, 8]. The identification, development and exploration of PET degrading enzymes has therefore become a research hotspot in efforts to advance the field [9, 10], yet they are currently constrained by the challenges of screening proteins for catalytic activity towards PET at a broader scale [11]. Current methods rely heavily in the detection of the polymer monomers terephthalic acid (TPA) and ethylene glycol (EG), or smaller units such as mono(2-hydroxyethyl) terephthalate (MHET), using sophisticated and costly instrumentation, such as high-performance liquid chromatography (HPLC) and mass spectrometry (MS). While highly sensitive, HPLC and similar techniques are primarily limited by their low-throughput and required expertise, halting the discovery and characterization of new proteins. [11, 12]. The development of new assays addressing these limitations is therefore needed for faster development of the field, and has been the focus of recent research [11, 13, 14]. Due to the hydrophobic aspect of PET, however, both traditional and novel assays are often designed to monitor only the final stages of PET degradation into water soluble products. As a result, enzymatic or catalytic activities that do not result in full depolymerization remain overlooked [15]. The development of an assay for catalytic activity using carbon dots (CD) as a fluorescent reporter of PET degradation aims to offer a more accessible and time-efficient approach to screening proteins for catalytic activity. The premise of the method lies in the release of a detectable fluorescent signal resulting from the degradation of a polymer matrix with CDs embedded therein. The method could reduce the need for costly instrumentation

but also allow for the identification of enzymes that may not fully depolymerize PET but still exhibit catalytic activity. Additionally, CD's advantageous properties, including small size, high hydrophilicity, non-toxicity, and ease of production make them an attractive option for widespread use. CD can be synthesized from a variety of readily available materials using simple techniques such as microwave-assisted pyrolisis, allowing for scalable production at low cost [16]. The proposed assay could therefore contribute to overcoming current bottlenecks in enzymatic degradation studies, potentially accelerating biorecycling advancements.

Theory 2

2.1 Photoluminescence and fluorescence

Photoluminescence (PL) is a process that results in light emission following the absorption of photons by a material. The term PL encompasses both fluorescence and phosphorescence, with the key difference lying in the excited state from which the molecule emits a photon. At the heart of fluorescence lies the concept of HOMO-LUMO transitions, where electrons transition from the Highest Occupied Molecular Orbital (HOMO) to the Lowest Unoccupied Molecular Orbital (LUMO). Upon absorbing the energy from a photon, an electron in the HOMO transitions to the LUMO, creating an excited-state molecule. After rapid relaxation to the lowest vibrational level of the excited state, the electron returns to the ground state by emitting a photon, resulting in fluorescence. The difference in energy between the HOMO and LUMO is directly related to the wavelength of the emitted light. The process is non-destructive to the material and can occur repeatedly, which is one of the key aspects of the applicability of fluorescent particles. Historically, fluorescence has been studied since the mid-19th century, with early researchers such as George Stokes and Sir William Herschel exploring its potential applications [17]. Fluorescence is typically a faster process, with emission occurring on the order of nanoseconds to microseconds, while phosphorescence involves a delayed emission often persisting after the excitation is stopped. The difference in emission time is explained by the pathway by which molecules return to their ground state (S_0) after absorbing a photon, typically illustrated by a Jablonski diagram as shown in Figure 2.1. Both the fluorescence and phosphorescence processes start with the absorption of a photon ($h\upsilon_A$), causing an electron to shift from the ground state S_0 towards an excited state S_1 or S_2. Fluorescence ($h\upsilon_F$) occurs when a molecule returns to the ground state by emitting a photon from from excited states of same spin multiplicity as the ground state (S_2 and S_1), releasing the excess energy in the form of light. Other energy dissipation process such as vibrational relaxation (VR) and internal conversion (IC), however, are faster than $h\upsilon_F$, causing the energy released as photon by fluorescence to be lower than that which was absorbed. This phenomena is known as the Stokes shift, where the dissipation of energy by light emission occurs in longer wavelength of lower frequency than that of the absorbed photon.

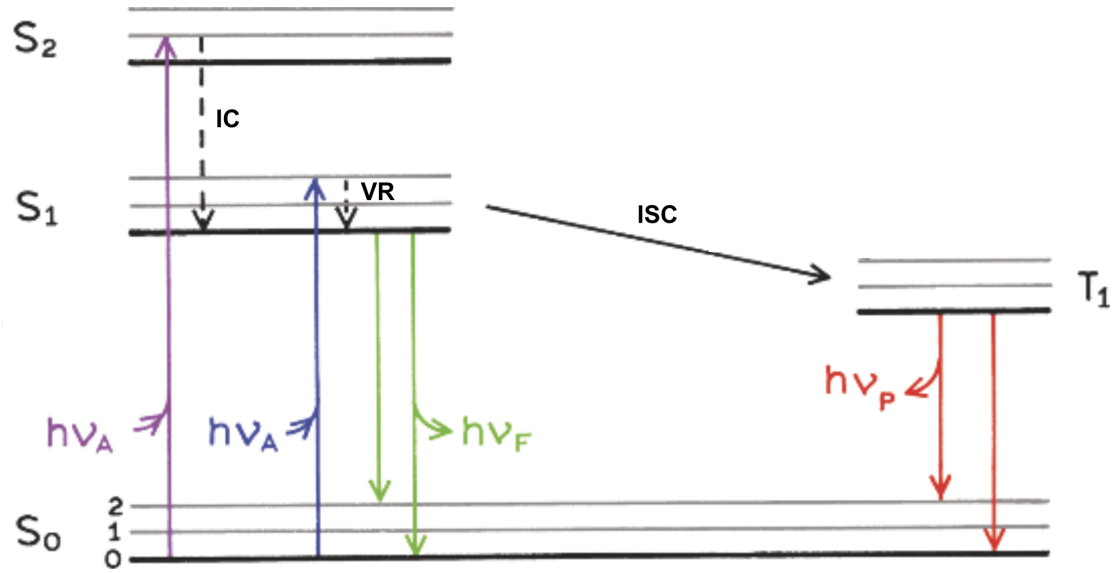

Figure 2.1: Jablonski diagram illustrating the energy transitions leading to fluorescence and phosphorescence. Absorption, fluorescence and phosphorescence are respectively indicated by Hv_A, Hv_F, Hv_P. IC: internal conversion; VR: vibrational relaxation; ISC: intersystem crossing. Figure adapted from [17]

Upon excitation, the molecule may initially reach a higher vibrational levels of an excited electronic state, illustrated in Figure 2.1 by the thin lines horizontal lines. In this case, the molecule undergoes VR, where excess vibrational energy is transferred either to other vibrational modes within the same molecule or to the surrounding molecules. This energy transfer causes the molecule to relax to the lowest vibrational level of the excited electronic state. Once the molecule has relaxed to the lowest vibrational level of a higher excitation singlet state (S_2), it may undergo internal conversion, where the molecule transitions to a lower excited state (S_1) of the same spin multiplicity. This transition happens because the vibrational levels of the two singlet states overlap, allowing energy to be transferred into vibrational modes. After IC from S_2 to a vibrational mode of S_1, the molecule may undergo further VR, returning to the lowest vibrational level of S1, at which fluorescence occurs. Phosphorescence, in the other hand, occurs in molecules which allow intersystem crossing (ISC), where instead of returning to the ground state via fluorescence, the molecule transitions into a triplet state (T1). This process results from a change in the electron's spin orientation from single state paired spins to the triplet state with unpaired, parallel spins. Once in T1, the molecule can return to S0 by emitting a photon via phosphorescence (hv_P). However, this transition is spin-forbidden as it requires a change in spin in order to transition back to the S_0 paired state and therfore takes longer to occur, leading to a delayed emission of light [17, 18]. Over the decades, the understanding of fluorescence has expanded, making fluorescence indispensable in chemistry and biological assays, where small quantities of substances can be rapidly detected based on their fluorescent properties. Advances in nanotechnology have laid ground for the development of new fluorescent materials such as carbon dots.

2.2 Electrospinning of Polymer Fibers

Electrospinning is a versatile technique used to fabricate fibers from polymer solutions or melts through the application of a high-voltage electric field. It has become widely used due to its ability to produce fibers with diameters in the nanometer scale with applications such as tissue engineering, filtration, and drug delivery [19]. The basic setup for electrospinning consists of syringe pump, a metallic needle through which the polymer melt is pumped, a high voltage power supply connected to the metallic needle and a grounded conductive collector towards which the solution is spun into fibers. The electrospinning process starts with the application of a high voltage to the metallic needle, charging the loaded polymer solution therein. The drop on the tip of the needle is subject to the electrostatic repulsion of the accumulated induced charges and to the external electric field created between the charged needle and the grounded collector. These forces distort the polymer droplet into a conical shape know as the Talyor cone, named after Sir Geoffrey Ingram Taylor, who first provided a theoretical explanation for the observed conical distortion of fluids under an electric field [19, 20]. By increasing the voltage past a critical point, the electrostatic forces overcome the surface tension of the liquid, causing it to be expelled in a jet from the tip of the Taylor cone. The jet follows the electric field towards the grounded collector, during which it is elongated and its surface area increases, thereby favoring solvent evaporation. The distance between the needle and the collector is set as such that the travel path allows for the evaporation of most of the solvent, resulting in the solidification of the polymer as thin fibers [19, 21].

The morphology and diameter of the fibers produced are influenced by a collection of factors, including proprieties intrinsic to the solution such as polymer concentration, conductivity and surface tension, as well as experimental conditions such as ambient humidity and temperature. The composition of the polymer solution have a direct effect in the stability of the jet, related to the balance between the opposing forces of surface tension and electrostatic repulsion acting on it. Surface tension tends to reduce surface area and can lead to breaking the jet into spherical beads while electrostatic repulsion favors the increase of surface area by elongation of the jet. Other characteristics of the solution contribute to this balance, such as viscosity. Low-viscosity solutions enable greater jet elongation, producing thinner fibers, but at the cost of stability, which can lead to bead formation as surface tension dominates [19]. In contrast, high-viscosity solutions stabilize the jet, reducing the likelihood of bead formation by resisting jet breakup, though the fibers tend to be slightly thicker due to less elongation [22]. Another example is the solvent conductivity, which promotes the electrostatic repulsion leading to thinner fibers by favoring the elongation of the jet [19]. The effect of humidity and temperature on fiber morphology, in the other hand, originates from their influence on solvent evaporation. High humidity levels can lead to the rapid condensation of water molecules onto the polymer jet as it travels toward the collector. This phenomenon can disrupt the uniform evaporation of the solvent, resulting in fiber defects such as beads, pores, or irregular surface structures. Conversely, low humidity levels may lead to too rapid evaporation of the solvent, causing fibers to become brittle and prone to breakage during deposition [22]. Humidity and temperature also significantly impact fiber morphology through their influence on solvent evaporation. At high humidity levels, water molecules can condense onto the polymer

jet, causing defects such as fiber fusion or pore formation. Temperature, on the other hand, accelerates solvent evaporation, favoring faster jet solidification and thicker fibers, although the decreased viscosity also promote finer fibers by increasing jet elongation [19, 22]. The results of electrospinning are therefore governed by a delicate balance between multiple factors, including solution properties, experimental conditions and environmental conditions. The parameters can be optimized towards a wide-variety of outcomes in fiber morphology and diameter, leading to the high versatility and vast applications of the technique [21].

Methods 3

3.1 Preparation and Characterization of Carbon Dots

Three different carbon dots (CDs) with distinct fluorescent properties were synthesized, arbitrarily referred to as CD1, CD2 and CD3. The synthesis were made via pyrolysis using a common microwave at 650 W for four minutes. CD3 was synthesized from a 5 mL suspension containing 0.5 g citric acid monohydrate and 386.6 mg diethanolamine. CD1 and CD2 were prepared from citric acid and urea at mass ratios of 0.2:1 and 2:1 urea to citric acid, respectively. Post-pyrolysis, the CDs were suspended in Milli-Q water and put in a sonic bath for one hour. The suspension was then centrifuged at 3000 rpm for 20 min, and only the supernatant was retained. Ultraviolet-Visible (UV-Vis) spectroscopy was performed to record the light absorbance of the CDs using a Shimadzu UV-1800 spectrophotometer, in the range of 300 nm to 600 nm. The wavelength of maximal absorbance for each CD was used for excitation during emission spectroscopy, which was conducted using an ISS Chronos DFD fluorescence lifetime spectrometer coupled to an ISS K520 digital frequency domain and a P110 lamp power supply. Emission measurements were made by scanning in 1 nm steps for 0.3 s without wavelength filters between the sample and the light source, measurements were made on samples diluted by a factor $1:500$ from each stock. Following qualitative inspection of CD fluorescence, dynamic light scattering (DLS) measurements were performed only for CD2 using a Brookhaven NanoBrook Series instrument and BIC Particle Solutions software. The DLS settings used were:instrument parameters at 90°, measurement temperature at 25 °C, set 30 s, equilibration time of 30 s, and particle size range of 10 nm to 50 nm. Ten automated measurements were taken with 0 s intervals, and a refractive index of 1.693 was used for the sample parameters [23]. The CDs were later lyophilized for storage. After initial comparison, CD2 was selected for further experimentation. Two additional batches of CD2 were produced following the same protocol and were verified for consistency by measuring absorbance, emission, and particle size using the herein described methods.

3.2 Preparation and Characterisation of PET films

3.2.1 PET film fabrication

PET films containing CD1, CD2 and CD3 were produced by spincoating. Serial dilution of the CD stocks in the orders of $1:10, 1:100, 1:1000, 1:5000$ were combined with a solution of 2% (w/v) PET pellets, dissolved in a mixture of 40% (v/v) dichloromethane (DCM) and 60% (v/v) trifluoroacetic acid (TFA). The mixture was stirred overnight at the lowest magnet rotation speed prior to the addition of CDs. Silicon wafers measuring 1 x 1 cm were covered with the PET-CD solution and spincoated at 8000 rpm for 90 s using a

POLOS SPIN150i spincoater. The films produced were screened for inclusion of CD using a312 nm UV lamp.

3.2.2 Fluorescence measurement of PET films

Emission spectroscopy measurements were attempted on films by fixating the films perpendicular to the light source, with a pivoting support allowing the angle between the light source and film to be adjusted to 30°, 45° or 60°.

3.2.3 pH and temperature testing on PET films

CD2-enriched PET films behaviour resulting from pH and temperature variation was investigated using PET films prepared with the 1 : 100 CD2 stock dilution. CD2-enriched PET films were incubated with 100 µL of 20 mMTris-HCl buffer deposited on their surface with pH values ranging from pH 5 to pH 8 by steps of 1. One set of experiments was carried out at room temperature and another at 60 °C, both sets had their fluorescent signal visually inspected for fluorescence with a 312 nm UV lamp after incubation. Effects of temperature increase were isolated by incubating two plain CD2-enriched PET films at 60 °C. One film was incubated for 20 hours, while the other was analysed after 2 hours. At the end of incubation times, both samples were rinsed with 200 µL MiliQ water. The rinsing volume as collected and inspected together with the films using a 312 nm UV lamp.

3.2.4 PET film working temperature range

The working temperature range of CD2-enriched PET films was investigated by incubating PET films for 24 hours in temperatures ranging from 30 °C to 60 °C in 10 °C steps. The experiment was conducted in duplicate: one set was incubated dry, the other set was incubated with 100 µL deposition of 20 mM TrisHCl (pH 8) on the films surface. After incubation time, all samples were rinsed with 200 µL MiliQ water which was collected for analysis.

3.2.5 Complementary qualitative testing

Visual qualitative inspections of fluorescence under 312 nm UV lamp were conducted: (I) CD2-enriched PET films were redissolved in 40% (v/v) DCM and 60% (v/v) TFA and then inspected for fluorescence; (II) CD2 dilution used for PET-film fabrication was heated to 100 °C over 10 minutes and inspected for fluorescence; (III) Mechanical abrasion was manually applied with metal spatulas to CD2-enriched PET films submerged in 150 µL MiliQ water, and the sumberging volume was collected after 2 minutes for fluorescence inspection. Prior to the abrasion, the PET films had been hydrated for 2 minutes with an equivalent volume, which had also been collected for analysis.

3.3 Preparation and Characterization of PET fibers

PET fibers were produced via electrospinning. Electrospinning was conducted with a Yflow Nanotechnology Solutions Electrospinner 2.2.D-500. Initial fibers were produced using solutions of 40% DCM (v/v) and 60% (v/v) TFA with 20% (w/v) dissolved PET pellets and 0.1% (v/v) CD2 stock. Starting for Fiber Assay 2, the solution used was adjusted

to 100% TFA with %25 (w/v) dissolved PET powder and 0.3% (w/v) lyophilized CD2. Inclusion of CD2 within the fibers was verified with a 312 nm UV lamp. The produced PET fibers were then taken to an Olympus IX71 fluorescence microscope for fluorescence signal imaging using a U-MWIB3 OLYMPUS Microscope Fluorescent Cube. The temperature dependence of the PET fibers fluorescence was evaluated by incubating similar PET fibers for 24 hours at 40 °C, 50 °C and 60 °C. All samples were visually inspected for fluorescence using a 312 nm UV lamp prior to heat exposure. Samples were rinsed with 150 µL MiliQ water post incubation before being re-inspected with a 312 nm UV lamp.

3.4 Catalytic activity assays

3.4.1 Assays on PET films

Peptide HF7 provided by Peter Fojan (Associate Professor, Department of Materials and Production) was deposited on CD-enriched PET films and incubated at 60 °C for 24 hours. A range of HF7 concentrations was tested using a serial dilution of factor 10 in TrisHCl buffer at pH 8.5, from 1 mM HF7 to 100 nM HF7. A volume of 100 µL of each dilution was deposited on different films which were then sealed within a large petri dish with parafilm. Each petri dish contained paper towels humidified with 15 mL of water in order to increase vapour pressure within the sealed environment. After incuabtion, 200 µL MiliQ water was pipetted onto the surface of each sample and then collected for analysis after one minute. Films were then rinsed with 5 mL and dried under nitrogen flow. All films and rinsing volumes were inspected under 312 nm UV lamp for visible fluorescent emission.

3.4.2 Assays on PET fibres

3.4.3 Fiber assay 1

The assay was conducted with Cutinase provided by Evamaria Petersen (Associate Professor, Department of Materials and Production) and aforementioned HF7 peptide on CD2-enriched PET fibers produced via electrospinning. The fibers were produced from a solution of 20% (w/v) dissolved PET pellets in 40% DCM (v/v) and 60% (v/v) TFA containing 0.1% (v/v) CD2 stock. Two parallel assays were conducted: (I) proteins applied directly onto fibers spun onto microscope glass slides (deposition assay); (II) pieces of PET fiber of same weight were cut out and immersed in Eppendorf tubes containing the proteins dissolved in buffer (immersion assay). The deposition assay was made with 100 µL of 40 µM Cutinase and 100 µL of 80 µM HF7 peptide. The immersion assay had proteins added in lower concentration as a compromise to the higher volume required and stock limitation: 400 µL of 10 µM Cutinase and 400 µL of 20 µM HF7 peptide. Both assays where conducted in 20 mM TrisHCl at pH 8 over 24 hours at 40 °C. Scanning Electron Microscope (SEM) images of the fiber sample after incubation were provided by Peter Kjær (Research Technician, Department of Materials and Production), who conducted the imaging using a Zeiss EVO 60 ESEM. The sample was coated with gold before imaging and images were taken at working distance of 8.5 mm, with 10 kV electron high tension.

3.4.4 Fiber assay 2

Deposition assay using 100 µL of five different protein solutions and a buffer control on fibers produced by electrospining a solution of TFA with 25% dissolved PET powder and 0.3% (w/v) lyophilized CD. Assay was made using microscope glass slides with CD-enriched PET fibers, one slide incubated at 37 °C and the other at 60 °C, both for 24 hours. Slides were sealed with parafilm within a petri dish containing humidified paper towels to maintain vapour pressure. Six subsections were delimited in each slide using a metal spatula for deposition assay, respectively: 1. Control (20 mM TrisHCl pH 8) ; 2. Cutinase (40 µM) ; 3. estDZ3mut (0.8 µM) ; 4. estDZ3mut (1 mM) ; 5. HF7(200 µM) ; 6. HSH-25 (200 µM). After incubation, each subsection was rinsed with 200 µL MiliQ water and the rinsing volume was collected to be qualitatively inspected for fluorescence. Immersion assay with the same protein solutions was simultaneously conducted, using 5 mg cut-outs of CD-enriched PET fiber. The cut outs were inmersed in 400 µL protein solutions of equal concentration to that of deposition assay. After 24 hour incubation, 500 µL MiliQ water was added to each sample in order to conduct emission spectorscopy analysis. The dilution was necessary to attain appropriate volume compatible with the available cuvette usage.

3.4.5 Fiber assay 3

Deposition assay using 150 µL of the same proteins as Fiber assay 2, with different concentrations. Depositions were made on individual CD-enriched PET fibers of 2 cm^2 cut from the same fiber mat, and sealed with parafilm within petri dishes containing humidified paper towel for 24 hours at 40 °C. The concentrations used were, respectively: 1. Control (20 mM TrisHCl pH 8) ; 2. Cutinase (40 µM) ; 3. estDZ3mut (0.8 µM) ; 4. estDZ3mut (320 µM) ; 5. HF7(200 µM) ; 6. HSH-25 (200 µM). After incubation, fibers were transferred to eppendorfs with 1 mL MiliQ water and centrifuged for two minutes on a table-top microcentrifuge at 7000 RCF. The total volume was recovered and analyzed for fluorescent emission both qualitatively and by emission spectroscopy, recording the emission spectra resulting from excitation wavelength of 410 nm. The presence of PET degradation byproducts was investigated using reversed-phase high performance liquid chromatography (RP-HPLC).

3.4.6 Fiber Assay 4

Fiber Assay 4 involved two sets of deposition assays and two sets of immersion assays using CD-enriched PET fibers, similar to those used in Fiber Assay 3, but produced over a longer period to yield thicker fiber mats. Each cut-out's weight was measured before incubation for comparative dry weight analysis. Deposition assays used cut-outs weighing 9.27 ± 1.40 mg, while immersion assays used cut-outs weighing 7.29 ± 0.76 mg. In addition to the previously used protein solutions, Esterase DZ3 wild-type was also tested, resulting in six samples per set and a total of 24 samples. The solutions used per sample set were: 1. Control (20 mM Tris-HCl, pH 7.5); 2. HSH-25 (125 µM); 3. HF7 (100 µM); 4. estDZ3wt (2 µM); 5. estDZ3mut (2 µM); 6. Cutinase (40 µM).

In the deposition assay, 200 µL of each protein solution was applied to the respective cut-outs, which were then sealed with parafilm within petri dishes containing wet paper

towels. In the immersion assay, cut-outs were submerged in 1 mL of protein solution within Eppendorf tubes. All samples were incubated for 24 hours at 40 °C. One set from each experiment (12 samples) was pre-centrifuged with Milli-Q water before protein exposure, followed by qualitative evaluation of the water phase using a 312 nm UV-lamp to investigate possible CD-release bias due to centrifugation. After the incubation period, both sets of each assay were centrifuged as described for Fiber Assay 3. Post-incubation, all 24 cut-outs were dried for 24 hours at 37 °C and their weights were measured. The centrifugation supernatants were analyzed using emission spectroscopy and RP-HPLC.

3.5 Reversed-phase high performance liquid chromatography (RP-HPLC)

RC-HPLC was used to analyze the content of PET degradation products BHET (bis(2-Hydroxyethyl) terephthalate) and TPA (terephthalic acid) on liquid recovered from assays 3 and 4. Measurements were made with a ThermoFisher Scientific Dionex Ultimate 3000 HPLC connected to a analytical C18 column and absorbance monitored using a diode array detector. The system was run isocratically with 25% acetonitrile and 75% MiliQ water and flow rate of 1 mL min^{-1}. Samples were adjusted to system condition and loaded with an injection volume of 20 µL. Solutions of BHET 100 µM and TPA 100 µM were prepared and run through the column for reference, their retention time was used to match absorbance peak in chromatograms of the inspected assay results. Fiber Assay 4 had their samples filtered with 3 kDa centrifugal filter units before further analysis by HPLC. Deposition assay samples of Fiber Assay 4 were complementary analysed by Virender Kumar (Postdoc Fellow, PhD. Department of Chemistry and BioScience) using a different setting: increasing gradient of methaol in 0.1% formic acid, from 10% to 100% over 20 minutes and flow rate of 1 mL min^{-1}, at 40 °C. Samples were adjusted to 50% methanol prior to loading the injection volume of 2 µL and the methanol gradient increase was set to: 10% to 50% over five minutes, 50% to 100% over twelve minutes, 100% continuously for three minutes.

3.6 Cutinase production and purification

Cutinase expression was conducted in Luria Broth (LB) containing ampicillin (100 mL^{-1}) at 25 °C using PFCEX1 plasmids in *E. Coli* BL21(DE3). Protein expression was induced at OD_{600} 0.8 for 6 hours with 0.3 mM isopropyl-β-d-thiogalactopyranoside (IPTG). TES buffer containing 20% sucrose was used to isolate the cutinase from the bacteria's periplasmic space via osmotic shock. The cells were centrifuged at 4 °C and resuspended first in TES then in MiliQ water. The supernatants were dialysed against water using 12-14 kDa MWCO dialysis tubes (Spectra/Por) and then adjusted to 20 mM NaAc (pH 5). A cation exchange column chromatography was conducted using 20 mM NaAc (pH 5) as equilibration buffer and an increasing gradient of 0 M to 1 M NaCl was used to elute the protein. The purified cutinase was diaylysed against water and freeze-dried.

3.7 SDS-PAGE

SDS-Page was conducted using stacking gels (12%) and separation gels (4%) described by Laemmli [24]. Protein samples were mixed with Laemmli sample buffer in a 1:1 ration and a heat shock was applied by 3 min incubation at 80 °C followed by 1 min rest on ice. Tris-Glycine-SDS (TGS) buffer was used for the electrophoresis, with a potential of 130 V, followed by biosave coomasie blue staining.

3.8 Materials

Dichloromethane and Acetonitrile were purchased from VWR LIFE SCIENCE. Trifluoroacetic acid was supplied from Iris Biotech and Polyethylene terephthalate powder and pellets from GoodFellow. Cirtric Acid, Bis(2-hydroxyethyl) terephthalate, terephthalic acid, Trizma base and Urea were purchased from Sigma Aldrich. All materials were used without further purification.

Results and discussion 4

4.1 CD synthesis and photoluminescence characterisation

Three recipes for CD production were used for CD synthesis, hereby referred to as CD1, CD2, and CD3, based on reported studies of well characterised CD [25–29]. All three different CD were successfully produced and showed different photoluminescent properties when excited with a 314 nm UV lamp. Specifically, CD3 showed visible fluorescence within the red wavelength range, CD1 showed visible fluorescence within the blue wavelength range, and CD2 showed visible fluorescence within the green wavelength range. Their light absorbance was analysed by UV-spectroscopy and showed a maxima at 342 nm, 410 nm, and 308 nm respectively for CD1, CD2, and CD3. These maxima in absorbance were then used to obtain the fluorescence emission spectra of each CD respective to their maximal absorbance, as presented in Figure 4.1.

The CD's emission spectra allowed for the characterisation of their photoluminscent profile as well as the quantified comparison of their fluorescent output. Both CD1 and CD2 yielded emission signals with intensity on order of magnitude higher than that of CD3. To determine the relation of excitation wavelength to fluorescence emission, the reverse approach was used by fixing the emission wavelength measured and varying the excitation wavelength applied. The fixed wavelength of emission measured was set to each corresponding emission maxima presented in Figure 4.1, i.e. 421 nm, 452 nm and 529 nm respectively for CD3, CD1 and CD2. The resulting excitation spectra are presented in Figure 4.2.

Out of the three produced CDs, CD1 and CD2 seemingly outperformed CD3 presenting emission and excitation spectra of the same magnitude (respectively Figs. 4.1b, 4.1c and Figs.4.2b,4.2c) and were consequently plotted together in Figure 4.3 for better contrast.
Their fluorescence was quantified using Fluorescence Regional Integration (FRI) by integrating the area corresponding to signal intensities exceeding an arbitrary threshold of 10^5 arbitrary units (au) [30]. In Figure 4.3a, CD1 shows higher FRI across a larger spam of wavelengths when excited at it's maxima absorbance wavelength than CD2. In Figure 4.3b, however, CD2 show to be less reliant on the specificity of the excitation wavelength, providing higher FRI across a broader spam of excitation wavelengths. These differences are relevant because CDs photoluminescent properties are know to vary based on surface passivation and surrounding environment [31, 32].
Although no passivation was directly applied to the CDs, embedding them within PET substrates could affect such properties, favoring the choice for CD2 as reporter molecule due to the lesser excitation specificity of its photoluminescent profile.

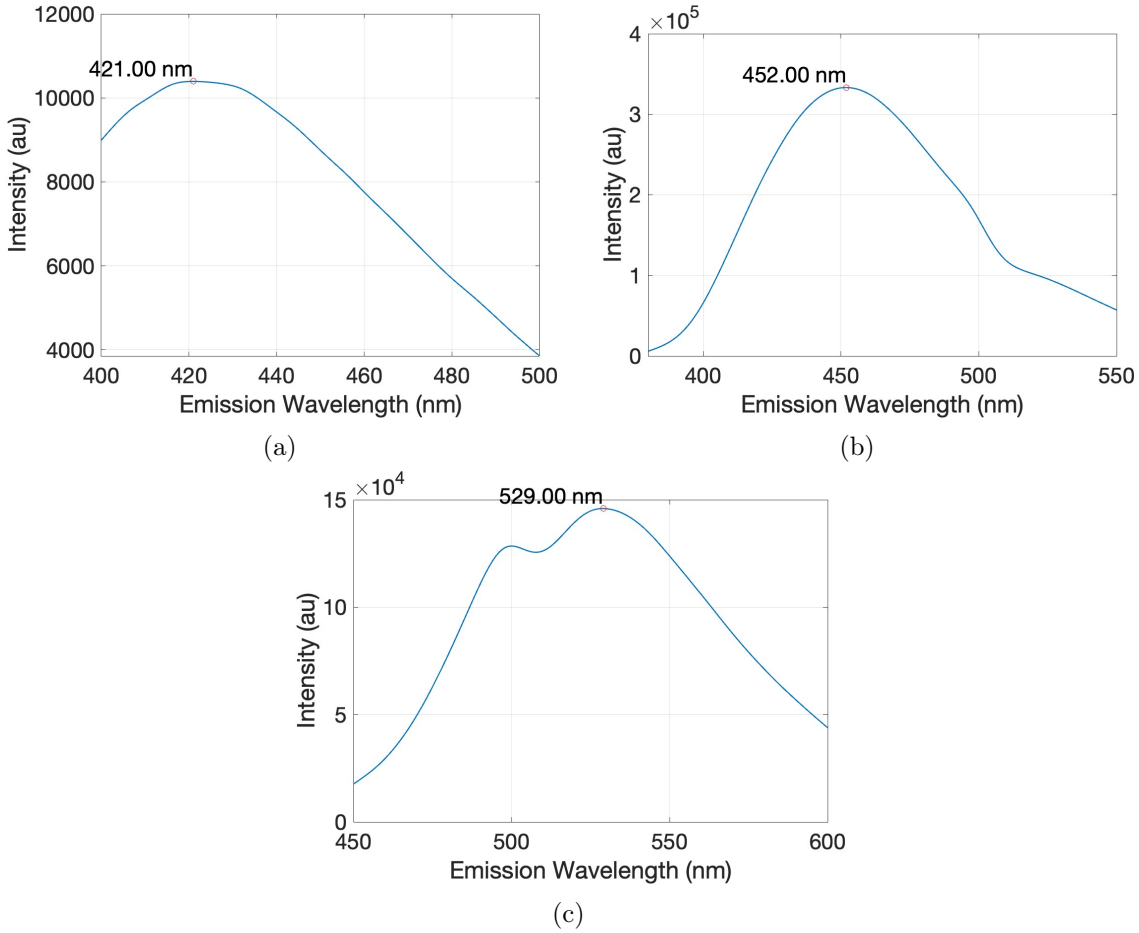

Figure 4.1: Fluorescence emission spectra of the three CDs. (a) CD3 emission spectrum for 308 nm excitation wavelength, maximum at 421 nm ; (b) CD1 emission spectrum for 342 nm excitation wavelength, maximum at 452 nm; (c) CD2 emission spectra for 410 nm excitation wavelength, maximum at 529 nm.

Finally, dynamic light scattering (DLS) was used to estimate the size of the produced CDs using samples at a dilution ratio of 1 : 100 from the originally produced stock. The particle's estimated diameters based on five consecutive measurements were of 396 ± 122 nm for CD1 and 21 ± 11 nm for CD2. Only three of the five measurements were used to estimate CD3 77 ± 27 nm due to outliers in the µm range, which were disregarded. Estimations for CD2 were in agreement with those measured by Qu *et al.* [29] using transmission electron microscopy and atomic force microscopy, but not for CD1 which was reported measuring between 4 nm to 45 nm. Moreover, later DLS estimations of CD2 diameter measured at a second point in time using ten consecutive measurements and two replicates yielded consistent results in contradiction to the first estimations, placing the average of CD2 estimated diameter at 185 nm, as shown in Figure 4.4.
The particle's photoluminescent properties were consequentially re-inspected after the difference in size estimations was measured, yet they presented the same characteristics as previously found. Increases in size estimations of CDs using DLS have been reported to be associated with long-term degradation of fluorescent impurities depositing on CDs over time [33] and were neglected in light of the consistent photoluminescent profile.

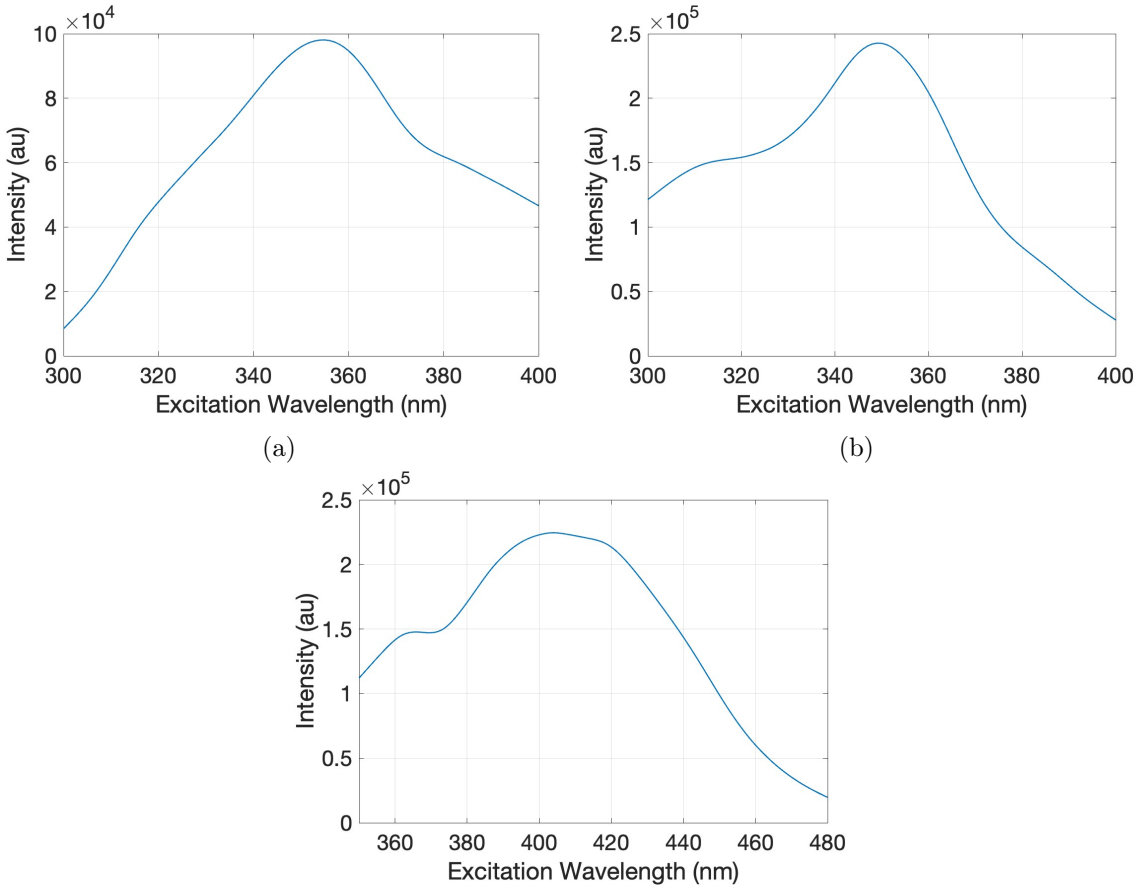

Figure 4.2: Excitation spectra of the three CDs. (a) CD3 excitation spectrum for 421 nm wavelength emission ; (b) CD1 excitation spectrum for 452 nm wavelength emission ; (c) CD2 excitation spectrum for 529 nm wavelength emission.

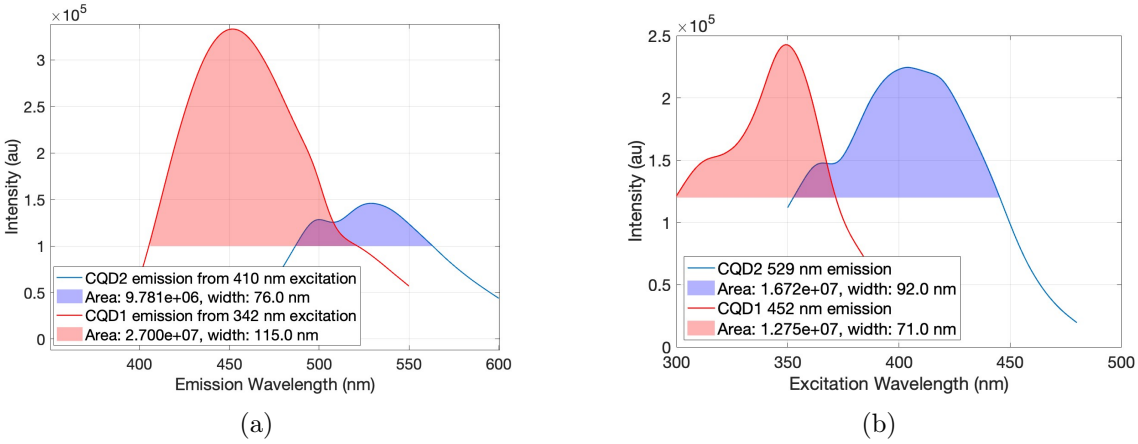

Figure 4.3: Comparison of CDQ1 (red) and CDQ2 (blue) photoluminescent properties. (a) emission spectra for CD1 and CD2, integrated for emission values higher than $1.2x10^5$ au ; (b) excitation spectra for CD1 and CD2, integrated for emission values higher than $1x10^5$ au

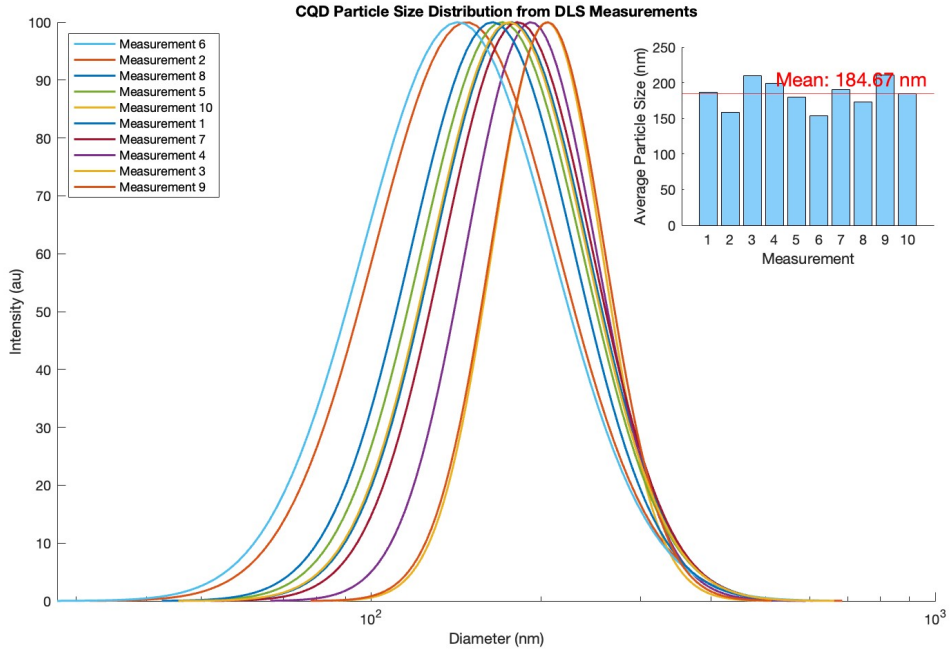

Figure 4.4: DLS distribution of CD2 measurements conducted at a second time, x-axis in logarithmic scale. Inset: Histogram of the mean diameter estimations from DLS measurement with a red line indicating the average mean diameter estimation at 184.67 nm

4.2 CD-PET composites

Initial attempts to integrate CD into a PET substrate were made by spincoating PET solutions containing CD into films. Given that CD are know to self-quench at high concentrations [34], PET films were prepared with different concentrations of CD, following a serial dilution from stock by factor 10. A concentration range for which the PET films presented fluorescent signal was identified between self-quenching and lower detection limit, as shown in Table 4.1. The fluorescent signal of the different PET films was compared semi-qualitatively based on visual inspection under a 312 nm UV lamp.

None of the PET films enriched with CD3 showed visible fluorescent signal upon qualitative inspection, while both PET films containing CD1 and CD2 showed clear fluorescence for dilution factors 1 : 100 and lower intensity fluorescence for dilution factor 1 : 1000. The absence of signal from CD3 within its corresponding PET films does not necessarily imply the complete absence of fluorescence but rather that no emission was perceived from the semi-qualitative evaluation.

Due to the inherently subjective nature of the semi-qualitative visual inspection, the difference in fluorescence intensity observed for PET films containing CD1 (++) and PET films containing CD2 (+++) at dilution 1 : 100 can not be directly associated with higher fluorescence emission from CD2. In fact, CD1 had reported comparatively higher fluorescent intensity at 312 nm excitation before integration into PET film (Figure 4.3a). The higher photolumincence attributed to PET films containing CD2 in Table 4.1 could therefore also result from a natural human perception bias in favor of green coloration in spite of similar emission intensity [35]. Efforts to quantify the fluorescence emission of the PET films were inconclusive. The CD-erniched PET films proved to be incompatible

with the fluorescence spectrometer, for fluorescence spectrometry measurements failed to detect emission signals from the PET films. The visual identification of fluorescence was therefore considered when selecting CD2 as the reporter molecule, as its clear visibility could improve the interpretation of semi-qualitative results."

Table 4.1: Semi-qualitative comparison of fluorescent emission in CD-enriched PET films with varying concentrations of different CD. Relative scale: (-) no observable fluorescence emission ; (+, ++, +++) progressively stronger observed fluorescence emission

CD concentration	CD1	CD2	CD3
Very high	-	-	-
High	++	+++	-
Medium	+	+	-
Low	-	-	-

4.3 Preliminary assessment of CD-enriched PET films

PET films prepared with CD2 (CD-enriched) were used for preliminary testing for the novel method o reporting catalytic activity based on substrate degradation. The HF7 peptide has been reported to degrade similar PET thin films at 65 °C with an optimal pH of 8.5 4.2 and was therefore chosen for the initial assessments of CD release induced by catalytic degradation of PET. Deposition assays (DA) were devised for this evaluation, in which 100 µL of Tris-HCl buffer (20 mM, pH 8.5) solutions containing the peptide HF7 were applied to the surfaces of CD-enriched PET films, as resumed in Table 4.2. The assays were designed on the premise that the highly hydrophilic CD entrapped within the PET films would leach from the hydrophobic substrate as a result of PET degradation, and a range of HF7 concentrations (0.1 µM to 1000 µM) was used in the attempt to measure a dose-dependent response fluorescent signal. A choice for semi-qualitative analysis was made given that previous attempts to obtain quantitative measurement of CD-enriched PET film fluorescence by fluorescence spectroscopy proved unsuccessful. The observed results, however, indicated a complete loss of substrate fluorescence with inconsistent evidence of CD leaching, as presented in Table 4.2, where only the sample incubated with 1 µM HF7 had a fluorescent signal observed in the deposited droplet when analysed post-incubation.

Table 4.2: Semi-qualitative inspection of fluorescence from CD-enriched PET films and corresponding supernatant after 20-hour incubation with HF7 peptide. PET films were incubated at 60 °C with 100 µL of HF7 peptide at varying concentrations in 20 mM Tris-HCl buffer, pH 8.5.

[HF7] peptide	PET film	Supernatant
1 mM	-	-
100 µM	-	-
10 µM	-	-
1 µM	-	++
100 nM	-	-

The inconsistent results of the DA brought forth the need to assess the robustness of CD-enriched PET films under varying experimental conditions of pH and temperature. The loss of photoluminescence across all substrates with one sole positive result for CD leaching on the deposited droplets prevented conclusions regarding the relation between

peptide activity and release of the reporter molecule. Nevertheless, the one positive result validates that the reporter molecules are not irreversibly entrapped within the substrate and can be transferred towards the deposited droplet.
Assessing the robustness of CD-enriched PET films under different pH and temperature conditions revealed the previously observed loss of substrate fluorescence to be temperature-dependent, and that the positive signal observed is not directly attributable to peptide activity (Table 4.3). PET films incubated with 20 mM Tris-HCl adjusted to pH in a range from pH 5 to pH 8 as a control experiment maintained fluorescence when incubated at room temperature while a parallel set incubated at 60 °C showed complete loss of photoluminescnce on par with previous results. Moreover, fluorescence quenching was observed in substrates after incubation at 60 °C, but fluorescence was restored when the quenched substrates were later dissolved in 40%/60% DCM/TFA (v/v), uggesting that temperature affected the PET films rather than the photoluminescent particles therein. Experiments conducted at a second time showed the CD-enriched PET films loss of fluorescence to follow a gradient with increasing temperature, with complete loss of signal at 50 °C (Table 4.4). From Table 4.3 it is observed that once again, one sample showed evidence of CD transferring from the substrate to the deposited droplet although in this case in the absence of peptide, suggesting that using CD leaching as a reliable reporter for catalytic activity required further substrate optimization. Further experimentation with CD-enriched PET films was therefore not pursued and a different approach using electorspinning to produce CD-enriched PET fibers was investigated instead.

Table 4.3: Semi-qualitative evaluation of pH and temperature effects on the fluorescence of CD-enriched PET films and associated CD release after incubation. PET films were incubated for 20 hours in 100 µL of 20 mM Tris-HCl buffer at the specified pH levels, with one set at room temperature and another at 60 °C.

pH	**Room Temperature**		**60°C**	
	PET film	**Supernatant**	**PET film**	**Supernatant**
ph5	++	-	-	++
ph6	++	-	-	-
ph7	++	-	-	-
ph8	++	-	-	-

4.4 Evaluation of CD-enriched PET Fibres

Electrospinning PET solutions containing CD was investigated as an alternative for the enriched PET films for the new screening method. Meshes of overlayed nanofibers produced by electrospinning are known to achieve high porosity and increased surface area [36], and were therefore produced in an attempt to facilitate protein interaction with the substrate. Electrospining a solution of 40%/60% DCM/TFA (v/v) containing 20% (w/v) dissolved PET pellets and 0.1% (v/v) CD2 stock yielded fluorescent fibers which were used for further analysis. Firstly, the enriched PET fibers were inspected with UV-microscopy and semi-qualitatively assessed for the temperature induced quenching effect observed for enriched PET films. The new substrate maintained fluorescence at temperatures up to 60 °C, as summarized in Table 4.4, and successfully incorporated CD into the fibers as shown in Figure 4.5. No CD leaching from either substrates was observed.

Table 4.4: Semi-qualitative evaluation of the fluorescence of CD-enriched PET films and electrospun PET fibres after incubation at the specified temperatures. Substrates incubated for 20 hours with 100 µL of Tris-HCl (20 mM, pH 8).

Temperature	PET film fluorescence	PET fibre fluorescence
30 °C	++	++
40 °C	+	++
50 °C	-	++
60 °C	-	++

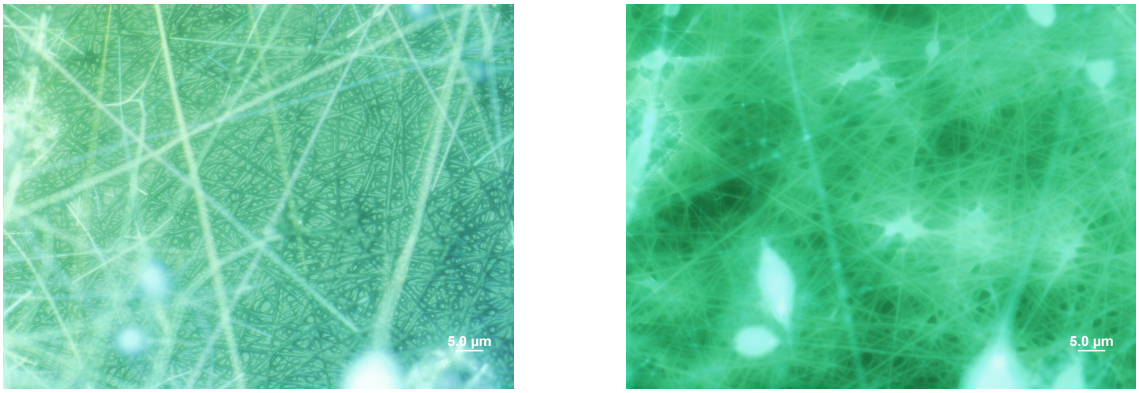

(a) (b)

Figure 4.5: UV-microscopy images of CD-enriched PET fibers. (a) Image obtained without wavelength filters (b) Fluorescence emission (510 nm to 550 nm) image of sample exposed to 460 nm to 495 nm excitation wavelengths

The fluorescent emission of the enriched PET fibers in Figure 4.5b was captured using a fluorescent cube composed of an excitation filter from 460 nm to 495 nm, an emission filter from 510 nm to 550 nm and a 505 nm dichroic mirror. The cube permits blue light to illuminate the sample, while only allowing green fluorescent light to reach the detector. Consequently, the resulting image exclusively captures the fluorescence emission (Figure 4.5b) of the enriched PET fibers. Interestingly, the excitation wavelength range permitted by the fluorescent cube corresponds to low intensity areas on the excitation spectra presented for CD2 (Figure 4.2c) and yet a clear fluorescent signal was produced, supporting the choice made for the reporter molecule with broader excitation spectra.

4.5 Catalytic activity assays on CD-enriched PET fibers

A series of assays based on catalytic activity were conducted to investigate the viability of the PET fibers containing CD as a substrate for the protein screening method. Each assay had adjustments made to either the substrate composition or the experiment conditions, with the goal of achieving a reliable correlation between CD release and PET degradation by catalytic activity.

4.5.1 Assay 1

The initial assay of this investigation was conducted using the HF7 peptide and *Fusarium solani pisi* cutinase, both of which are known to successfully cleave PET chains [37–40].

A deposition assay, similar to the one previously conducted with enriched PET films, was set up to assess rather alterations to the substrate caused by the HF7 and cutinase could be detected. The DA was conducted by exposing the CD-enriched PET fibers produced as previously described to HF7 (80 µM), cutinase (40 µM) and TrisHCl as a buffer control test (20 mM) for 24 hours at 40 °C. The fibers were inspected before and after incubation under a 312 nmUV lamp, as shown in Figure 4.6a To complement the investigation, an Immersion Assay (IA) was devised and conducted simultaneously where separate 2 cm^2 pieces of CD-enriched PET fibers were incubated in the same experimental conditions while submerged within 400 µL of 10 µM Cutinase, 20 µM HF7 and 20 mM TrisHCl. This assay focused in analysing the release of CD from the substrate by measuring the emission spectra of the solutions post incubation (Figure 4.6b). The different concentrations used in the parallel assays were due to limitations in the provided cutinase stock during testing. Nonetheless, both assays presented substrate degradation induced by cutinase, with DA results showing visible PET fiber removal and IA results showing close to three-fold increase of 535 nm emission for samples immersed in cutinase than for the control test (Figure 4.6). The assays failed to produce a clear response signal to HF7 degradation, with no visually detectable substrate alteration on DA and inconclusive increase in emission signal for IA as compared to control test. It was also observed that a fluorescent signal was obtained for the control test on IA, suggesting that detectable amounts of CD leak from the substrate regardless of catalytic activity.

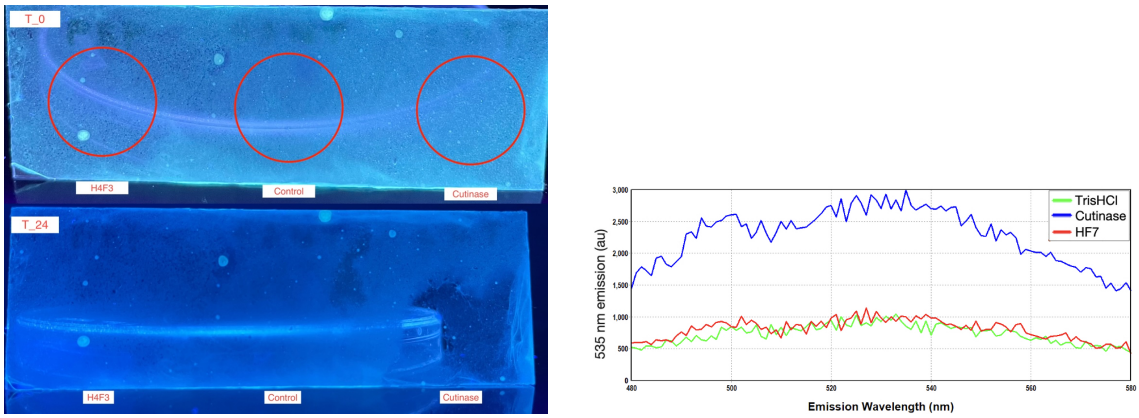

(a) (b)

Figure 4.6: Results from initial assays conducted on CD-enriched PET fibres. (a) Deposition assay substrate illuminated with a UV lamp set to 312 nm. top: substrate before assay, circles from left to right indicate areas to be covered respectively by HF7 peptide, TrisHCl and cutinase; bottom: substrate after assay.(b) Emission spectra measured from immersion assay after incubation.

The DA sample was further investigated by Scanning Electron Microscopy (SEM), revealing that the surface of the substrate exposed to HF7 also showed areas with degraded PET fibers, as presented in Figure 4.7c and 4.7d. The melt-like morphology observed in regions of PET nanofibers with pronounced HF7 activity (Figure 4.7d) could be attributed to partial cleavage of polymer chains within the amorphous regions of the PET fibers resulting in the accumulation of small insoluble oligomers at the surface. Polymer chains of small average molecular weight have been shown to have reduced glass transition temperature in other polymers [41]. The amorphous regions of polymers, characterized by

their disordered and flexible chain structure, become more mobile when molecular weight decreases, particularly when the glass transition temperature approaches the experimental temperature [42]. Furthermore, the cleavage of polymer chains without significant material removal could also account for the reduced CD release observed in the IA assay, as the reporter molecules remain entrapped within the substrate. This mechanism of partial degradation, therefore, provides a plausible explanation for both the melt-like morphology and the low CD release signal in the presence of HF7.

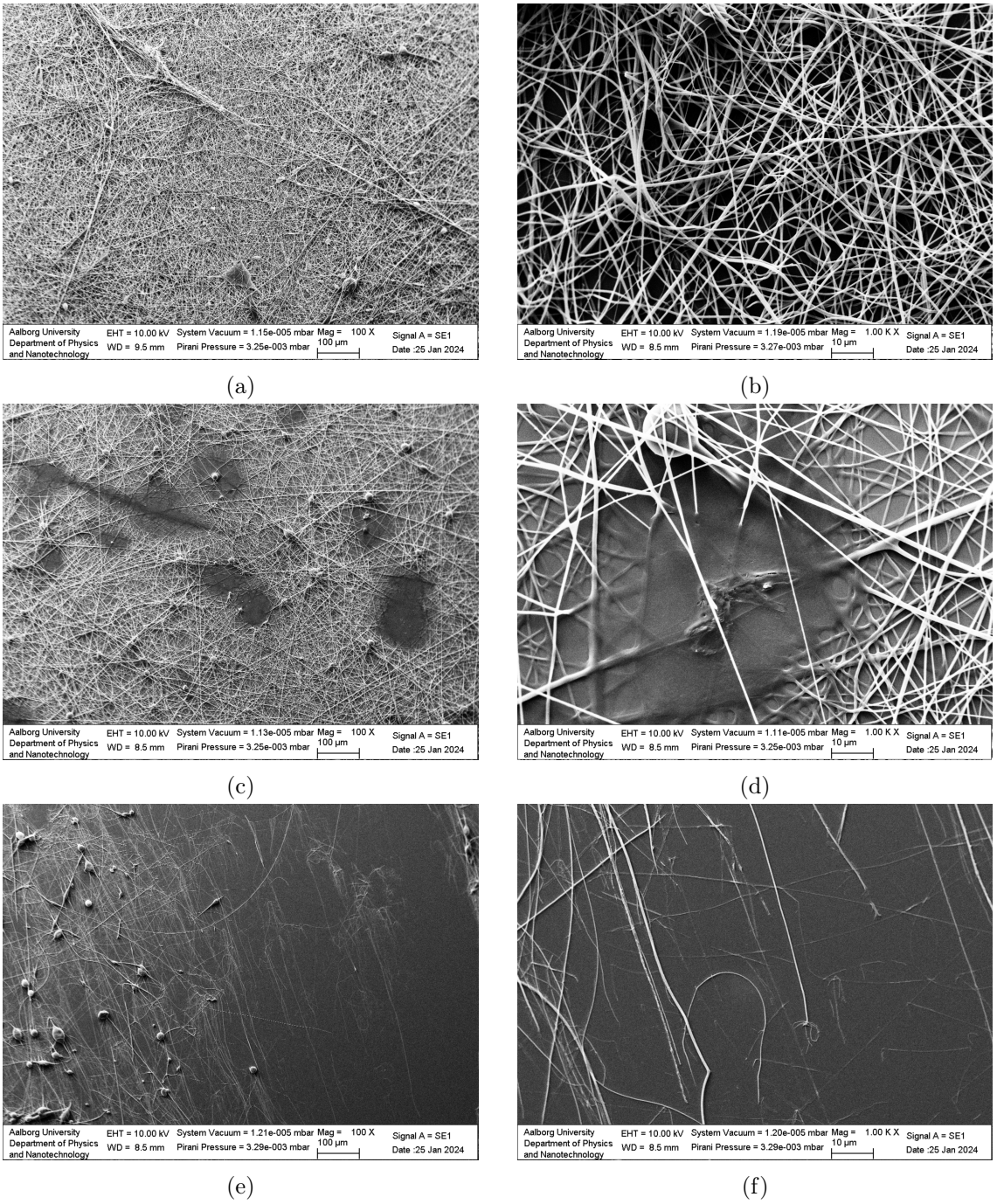

Figure 4.7: Scanning Electron Microscopy images of CD-enriched PET fibers on microscope slide, after incubation for 20 hours at 40 °C with (a,b) 20 mM TrisHCl; (c,d) 80 µM HF7 ; (e,f) 40 µM cutinase. The scale bars are 100 µm for (a, c, e) and 10 µm for (b, d, f)

4.5.2 Enzyme production

Following the depletion of the provided cutinase stock, cutinase expression and purification was conducted based on the procedure established for the expression of the provided cutinase [43]. SDS-PAGE was used to verify that the protein expression was successful before purification (Figure 4.8). Additionally, stocks provided for Esterase DZ3 (estDZ3wt) and Esterase DZ3 mutant I144F M203Y (EstDZ3mut) was simultaneously verified for their protein content.

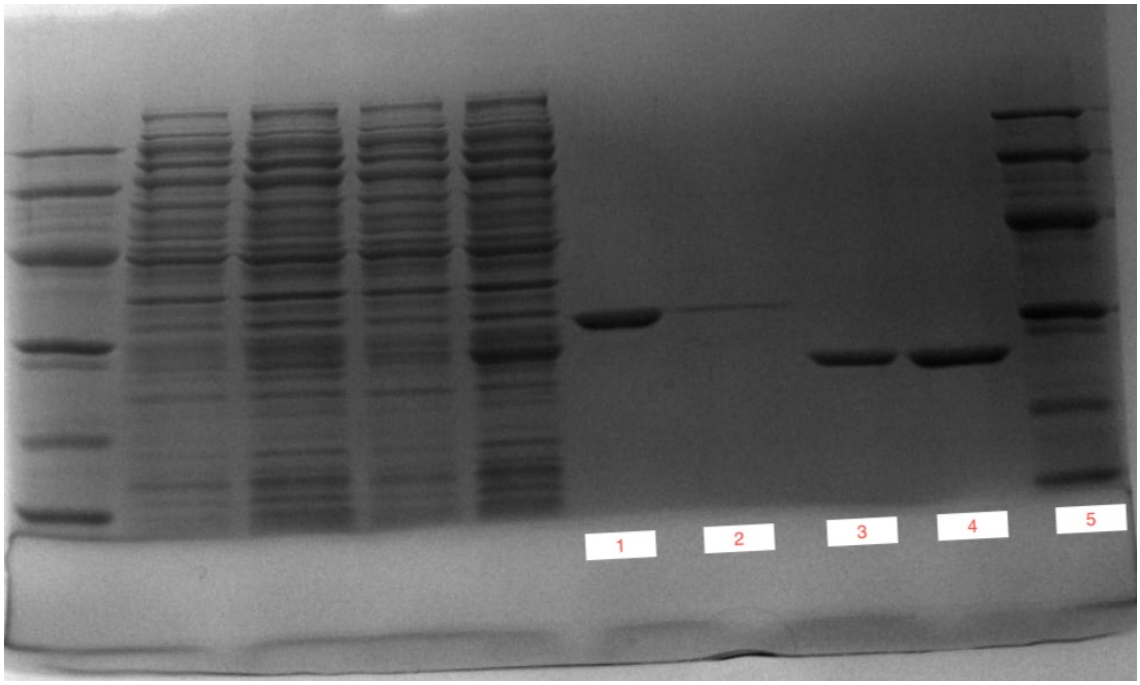

Figure 4.8: SDS-PAGE of fractions collected from cutinase expressions, and of enzyme stocks provided. From left to right: (1) estDZ3mut ; (2) estDZ3wt ; (3) TES fraction of produced cutinase ; (4) water fraction of produced cutinase ; (5) protein ladder. Samples to the left of the enumerated columns are not related to this work.

4.5.3 Assay 2

The SEM images were followed by a new set of DA and IA on a newly prepared substrate. The production of PET fibers was adjusted to electrospinning a solution of 25% (w/v) PET powder dissolved purely in TFA, containing 0.3% (w/v) CD. The original CD2 stock was lyophized to allow for the incorporation of the increased amount of CD within the PET fibers. The CD percentage of the polymer solution was increased in an attempt to amplify the intensity of florescence emission. The PET content of the electrospining solution was increased to reduce the solvent content, and the use of DCM was abandoned due to its toxicity. In addition, the list of reactants employed in the following assays was extended to include the peptide HSH-25 and the Esterase DZ3 I144F M203Y (EstDZ3mut) in order to explore the capability of the developing method to report the catalytic activity of other proteins. The former is a peptide designed for non-substrate specific hydrolysis of polyesters, which has been showed to degrade PET chains [44] while the latter is an enzyme optimized *in silico* for PET degradation, which has not been tested experimentally [45]. However, due to misleading concentrations on the provided estDZ3mut stock, the enzyme

concentrations used for the following assays were miscalculated. Corrected concentrations are shown in the following assays (Assay 2, 3 and 4), leading to unintended large variations between protein concentrations used, not allowing for direct comparisons. In order to address the previously inconclusive IA signal from HF7, the peptide concentration used in the new assay was increased to 200 µM. The new peptide tested, HSH-25, was adjusted to the same concentration (200 µM)to facilitate comparison while Cutinase concentration was maintained at 40 µM. Finally, estDZ3mut was used both at a high concentration (1 mM) and a low concentration (0.8 µM), given that its activity had not yet been experimentally characterized. Two equivalent DAs were conducted, one at 37 °C to maintain consistency with the previous assay, and one at 60 °C to enhance peptide reaction rates, as higher temperatures generally accelerate catalytic processes, according to the Arrhenius equation [46]. Microscope slides coated with CD-enriched PET fibers were divided into six sections, each exposed to a different reactant, including a control test with 20 mM TrisHCl at pH 8. After incubation it was found that the deposited reactants had come in contact with each other during incubation, proving the high compartmentalization of a single substrate to be unsuited for PET fibers on glass slides. The DA conducted at 37 °C showed direct contact between the reactants applied to the substrate, and was therefore disregarded of further analysis. The DA conducted at 60 °C showed an overlap of the diffusion radius for the different reactants, as indicated by dashed outlines in Figure 4.9a, but the remnant of the solutions deposited on the surface were clearly separated. The separated remnants were collected for qualitative inspection, as shown in Figure 4.9b. Due to the overlap of the diffusion radius, the fluorescence observed for the remnants collected could not be directly attributed to the different solutions applied to each section. The visibly distinct fluorescent intensities observed across the samples, however, suggest that a progressive release of CD as a function of catalytic activity could potentially be achieved.

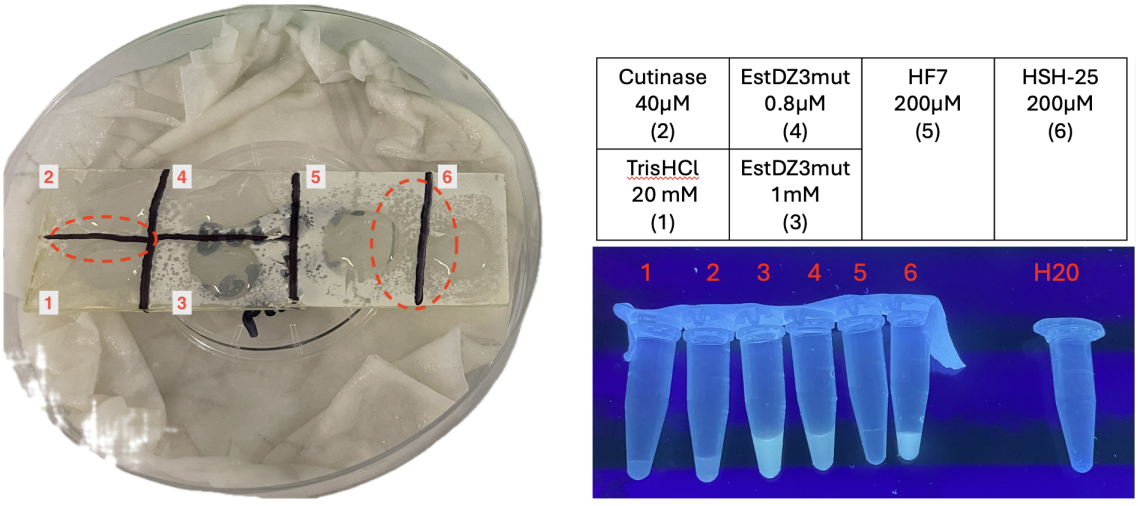

(a) (b)

Figure 4.9: Deposition assay conducted at 60 °C over 24 hours. (a) CD-enirched PET fibers divided into six sections, after incubation. Dashed outlines added to illustrate overlapping diffusion radius. Subsections are numerated according to deposited reactant: 1. TrisHCl 20 mM, 2. cutinase 40 µM, 3. estDZ3mut 1 mM, 4. estDZ3mut 0.8 µM, 5. HF7 200 µM, 6. HSH-25 200 µM ; (b) Top: shcematic representation of the deposition assay, bottom: remaining supernatant recovered form deposition assay, illuminated with a 312 nm UV lamp. Water sample added as non fluorescent reference.

The complementary IA was conducted with reactant concentrations adjusted to match that of the DAs and their results are presented in Figure 4.10. Both peptides HF7 and HSH-25 measured higher emission intensity outside of the expected maximal emission range for CD2 (500 nm to 550 nm). Specifically, HSH-25 emission at 460 nm showed a four-fold increase compared to the maximal emission intensity of cutinase at the expected range (Figure 4.10a). The fact that HF7 also showed an increase in emission at shorter wavelengths (4.10b), in contradiction with previous results, hints to a possible explanation related to higher peptide concentrations resulting in peptide-CD interactions. To this point, both peptides are primarily composed of histidines, which have been show to interact with CDs fluorescent properties [47, 48]. Moreover, the histidine content of HSH-25 is double that of HF7 and the peptide's has a natural propensity to aggregate resulting from its amphiphilic nature, both of which are factors that could contribute to the shift of the emission maxima and higher magnitude observed for HSH-25 emission. A new emission spectrum was recorded for HSH-25 after the sample was centrifuged for two minutes on a table-top microcentrifuge at 7000 RCF, and is presented in Figure 4.10c. The signal intensity of 460 nm emission signal is decreased four-fold, supporting the partial explanation based on CD-peptide interactions. Cutinase demonstrated a strong signal intensity at the expected CD2 emission maxima (550 nm). The consistent signal with previous IA results highlights its potential use as a positive control for the assay. Conversely, estDZ3mut exhibited higher emission intensity than the control test at low esterase concentrations but lower emission intensity at high esterase concentrations. It is unlikely that the lower signal originated from variations in CD leakage from the substrate because the PET fibers pieces of similar weight were used for IA. The lower emissions compared to the control test could result from dynamic quenching due to saturation of the sample, driven by the high protein concentration [49]. Additionally, CD quenching has been observed in glucose-based hydrogels due to esterase-substrate interactions, leading to CD aggregation within the degraded matrix [50]. Although a different substrate is used in this case, a possible quenching mechanism resulting from interactions between estDZ3mut and PET fibers could be present. To further investigate this effect, the maximal concentration of estDZ3mut was reduced in subsequent assays.

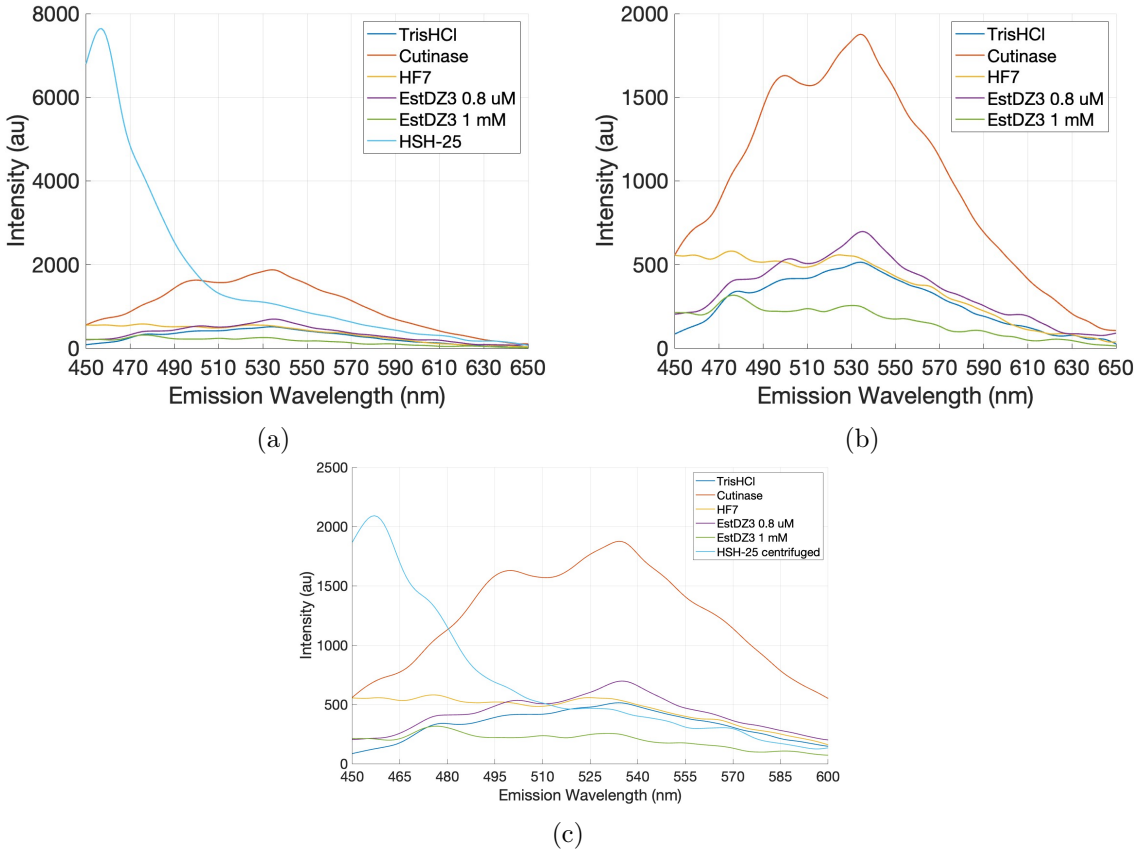

Figure 4.10: Emission spectra of the Immersion Assay conducted with TrisHCl 20 mM, cutinase 40 µM, estDZ3mut 0.8 µM, estDZ3mut 1 mM, HF7 200 µM and HSH-25 200 µM. (a) Plot displaying the spectra of all reactants ; (b) HSH-25 spectrum omitted ; (c) Spectra of all reactants and HSH-25 spectrum measured after centrifuging.

4.5.4 Assay 3

A third catalytic activity assay was conducted with the intention of improving the understanding of the previous results. The following adjustments were made to the procedure of the new assay: (I) Isolated substrates were used for each reactant given the limitations observed for substrate compartmentalization. Electrospinning was conducted over a longer period of time to produce a thicker, more manageable mat of PET fibers, which allowed 2 cm^2 sections to be easily cut for each sample. (II) The separated sections also allowed for the increase of the droplet volume deposited on the individual substrates to 150 µL as sample interaction via diffusion was no longer a restricting factor. (III) Reversed-phase high performance liquid chromatography (HPLC) analysis was conducted post-incubation to assess the presence of PET degradation products TPA and Bis(2-Hydroxyethyl) terephthalate (BHET). The analysis intended to investigate the relation between CD release and catalytic activity. (IV) After incubation, all substrates were submerged in 1 mL MilliQ water and centrifuged to avoid possible CD-protein aggregates and the supernatant was used for fluorescence spectometry and HPLC analysis. (V) Lastly, the upper-concentration of estDZ3mut used was reduced from 1 mM to 320 µM to investigate the quenching effect previously observed. The concentration of all other reactants was maintained equal to the previous assay. The fluorescence spectroscopy results respective to 410 nm excitation are presented in Figure 4.11a, the spectra show a

homogeneous profile across all samples, with variation in emission intensity. In comparison to the profiles obtained on the previous assay (Figure 4.10c), the profile of the emission spectra shown in Figure 4.11a have a higher similarity to that of the emission spectrum found for the characterisation of CD2 (Figure 4.1c). The similarity in profile suggests that the assay adjustments led to a better representation of the released CD available in the solution. The measured emission of each reactant relative to the control test, however, seems mostly unchanged across both assays with the exception of estDZ3mut. Reducing the tested upper-concentration for estDZ3mut from 1 mM to 320 µM failed to bring the resulting emission signal above that of the control test (TrisHCl), suggesting that the observed deficit in fluorescence as compared to the control test is not directly related to protein concentration. Moreover, the sample incubated with 0.8 µM also presented an emission deficit, contrary to the results of the previous assay, going against the dynamic quenching explanation for the observed effect. In the other hand, results from RP-HPLC suggest that PET degradation products are found in samples incubated with estDZ3mut, incidentally validating its activity towards PET (Figure 4.11c). Reference HPLC measurements of the PET degradation products TPA and BHET were made using 100 µM solutions, TPA showed a retention time of 5 mintues while the absorption peak associated to BHET is maximal at 6.5 minutes (Figure 4.11b).

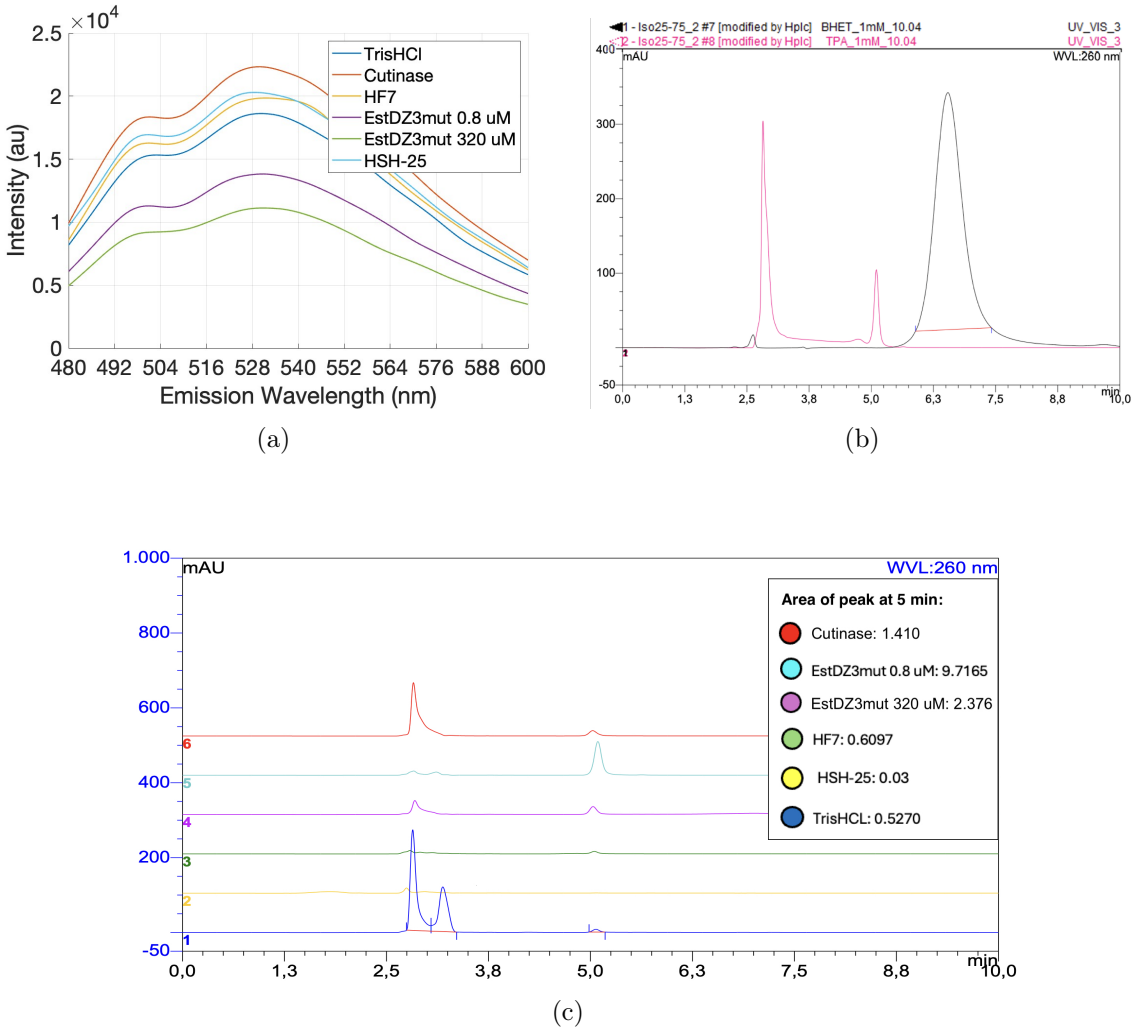

(a) (b)

(c)

Figure 4.11: Fluorescence spectroscpoy and RP-HPLC 260 nm chromatogram results from third assay. (a) Emission spectra of all centrifuged samples respective to 410 nm excitation; (b) RP-HPLC chromatogram of TPA (pink) and BHET (black) reference solutions depicting absorbance at 260 nm as a function of retention time. TPA and BHET peaks have their maxima respectively at 5 min and 6.5 min ; (c) Ensamble of RP-HPLC 260 nm chromatogram as a function of retention time for all samples. Individual chromatograms have been shifted along the y-axis for better visualisation. The color-coded inlet describes the area under the peak at 5 min for each corresponding sample

For RP-HPLC analysis, samples were adjusted to 25% acetonitrile and run isocratically through the column for a duration of 10 mintues. The chromatography results shows samples incubated with 40 µM cutinase, 320 µM estDZ3mut and 0.8 µM estDZ3mut to have an absorption peak at the same retention time observed for the TPA reference (Figure 4.11c), suggesting the presence of the degradation product within those samples. Moreover, the quantification of the area under the samples peak corresponding to the retention time of TPA suggests a higher amount of the degradation product within samples incubated with estDZ3mut than in that incubated with cutinase, in opposition to the trend of fluorescence emission repported by CD release (Figure 4.11a). The individual chromatography results of the enzymes for 214 nm, 230 nm, 260 nm and 280 nm wavelengths are presented for comparison in Figure 4.12, identified peaks have been annotated together with their

retention time, starting with injection peaks. At the retention time of the TPA reference, the three enzymes show absorption peaks for 230 nm and 260 nm wavelengths, characteristic of TPA absorption. The complementary wavelengths 214 nm and 280 nm are used to detect proteins, specifically peptide bonds and amines absorb at 214 nm while aromatic amino acids absorb at 280 nm. Both estDZ3mut samples show peaks for the mentioned wavelengths indicating that presence of proteins within the eultion of the peaks associated with PET degradation products, yet the magnitude of the absorption peaks for 230 nm and 260 nm together with the associated integrated area of 260 nm support the presence of TPA in higher amounts than observed for cutinase. Interestingly, the sample incubated with 320 µM estDZ3mut shows a third peak corresponding to the retention time of the BHET reference, suggesting that at higher concentrations the depolymerisation of PET into monomers. The fact that the estDZ3mut samples seem to present higher amount of PET degradation products but do not show a corresponding higher emission signal from released CD could suggest that the substrate release of the photoluminescent particles is not directly correlated to PET degradation.

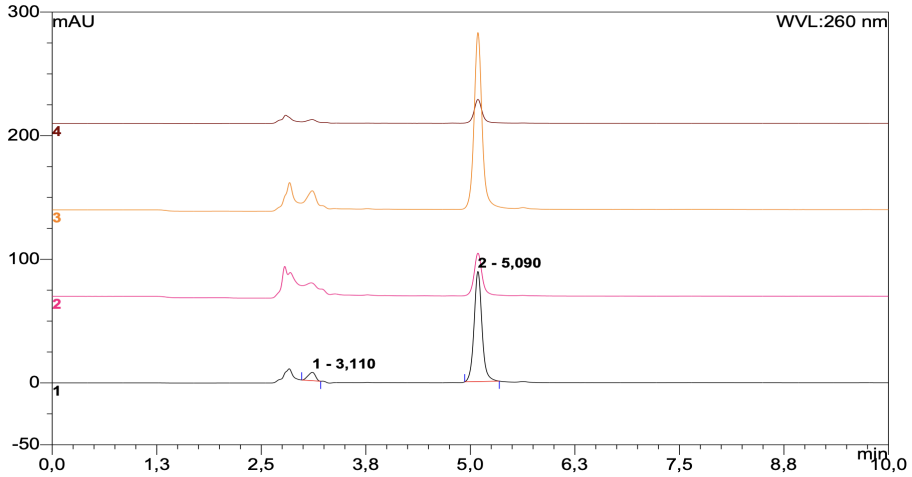

(a)

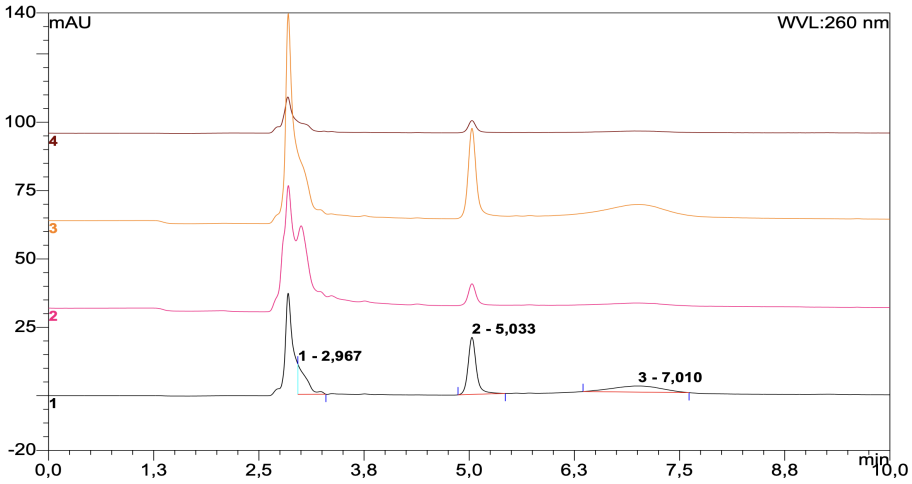

(b)

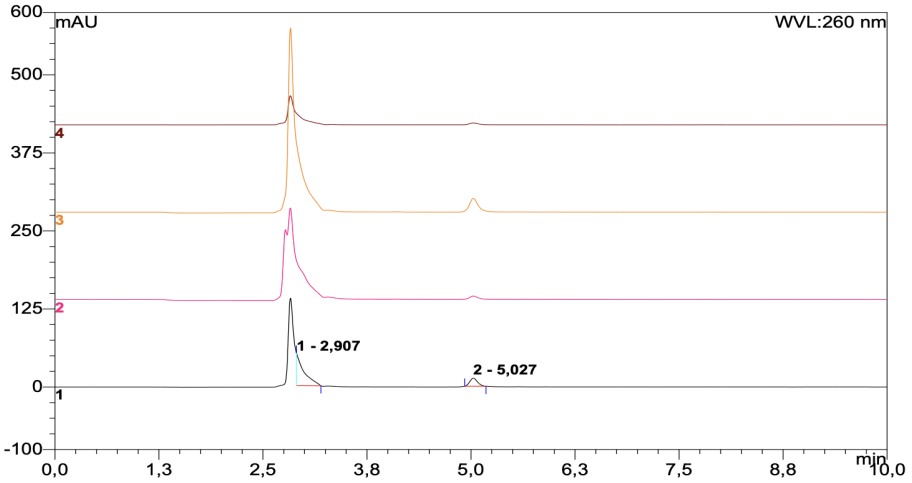

(c)

Figure 4.12: Individual RP-HPLC chromatogams of estDZ3mut and cutinase samples depicting absorbance of 214 nm (pink), 230 nm (orange), 260 nm (black) and 280 nm (brown) as a function of retention time. Y-axis scales correspond to 260 nm, other chromatograms have been shifted for better visualisation. (a) Chromatograms for 0.8 µM estDZ3mut ; (b) Chromatograms for 320 µM estDZ3mut ; (c) Chromatograms for 40 µM cutinase. Annotations within chromatograms innumerates measured peaks and displays the retention time of the respective maxima.

4.5.5 Assay 4

A fourth assay was conducted, divided in two distinct sets, Set I and Set II, and both DA and IA were conducted for each set. Substrates of Set II were centrifuged in MiliQ water before protein exposition in an attempt to reduce background noise from CD-leakage. Both sets were centrifuged post-incubation, following the procedure of Assay 3. Each set comprised 6 samples for DA and 6 samples for IA, totalling 24 samples which were inspected by HPLC and emission spectroscopy. The primary goals of Assay 4 were to replicate the results of Assay 3, determine whether centrifuging the substrates led to increased CD-leakage and investigate if centrifuging the substrates prior to incubation reduced background measurements. Assay 4 was devised so that the DA samples from Set II were the equivalent experiment of Assay 3, serving as a replicate for the previous assay. The peptide concentrations used in Assay 4, however, were adjusted to lower values due to stock limitation. Additionally, the wild-type of Esterase DZ3 (estDZ3wt) was included in Assay 4, as an attempt to provide a reference for evaluating estDZ3mut. The following concentrations were used for the six different incubation conditions: (1) control test (Tris-HCl 20 mM); (2) HSH-25 at 125 µM; (3) HF7 at 100 µM; (4) EstDZ3wt at 2 µM; (5) EstDZ3mut at 2 µM; (6) Cutinase at 40 µM.
Following incubation, IA samples which had been exposed to cutinase showed visually distinctive fluorescence emission in the supernatant for both Set I and Set II, as presented in Figure 4.13. The significant increase in fluorescence resulting from CD release in IA incubated with cutinase is also seen in the fluorescence spectrometry results, shown in Figure 4.14. Results from DA of both Set I and Set II also show a increased emission intensity resulting from cutinase incubation (Figure 4.15), albeit at lower intensity than their IA counterparts, suggesting that the assay reliably reports PET degradation resulting form cutinase activity. IA was not conducted for HSH-25 samples due to limited availability of peptide stock.

Figure 4.13: Both sets of IA samples examined over a 312 nm UV lamp after incubation. Left hand side: Set I; right hand side: Set II. Samples incubated with cutinase are indicated in red.

The emission spectra obtained for the other proteins offer limited insight into the assay performance, as no consistent trend is observed across the assays. The ensamble of their emission spectra seem to fluctuate around values measured for the TrisHCl control, not

allowing for distinctive conclusions to be made. Moreover, emission spectra from DA of Set I (Figure 4.15a) are not consistent with those measured in Assay 3 (Figure 4.11a), made under similar conditions, suggesting that the concentrations used for Assay 4 may be bellow the sensitivity of the assay for the tested proteins, with the exception of cutinase. The emission spectra measured for the TrisHCl control test showed to be consistent between IA results of Set I and Set II (Figures 4.14b and 4.14d, respectively) and showed little variation across DA results of Set I and Set II (Figures 4.15a and 4.15b, respectively), suggesting that centrifuging the substrate prior to protein incubation does not have a significant impact on CD leakage from the substrate. The difference of emission intensity measured for cutinase between IA and DA of both sets indicates that assays where the substrate is submerged in a protein solution result in a more distinct signal than assays where the enzyme is applied to the surface, which is to be expected given the increased coverage of the substrate surface. Nonetheless, DA results successfully reported an increased release of CD, suggesting that the method could also be suited for working with small volumes.

The HPLC results investigating the presence of TPA and BHET within the samples had to be disregarded due to issues with the instrument, involving column pressure above normal operating conditions and leakage from the injection valve (data not shown). The samples were therefore taken to the Department of Chemistry and BioScience for further HPLC analysis. The provided HPLC analysis was conducted using a different methodology, where peaks associated with TPA detection were found for cutinase samples and for HSH-25 samples, as presented in Figure 4.16. The HPLC analysis was conducted exclusively for samples from Set I, due to the availability of the department. The sample incubated with HSH-25 from Set II was exceptionally added to the HPLC analysis (Figure 4.16b) in order to avoid having only one result from HSH-25 incubation analysed. The comparison of the HPLC analysis results (Figure 4.16) with those from fluorescence spectrometry (Figures 4.15 and 4.14a) supports that Assay 4 successfully reported PET degradation resulting from cutinase incubation. However, it also suggests that the assay failed to report PET degradation resulting from HSH-25 incubation, indicating that further optimization is required before the assay can reliable be applied for proteins whose optimal conditions are not known.

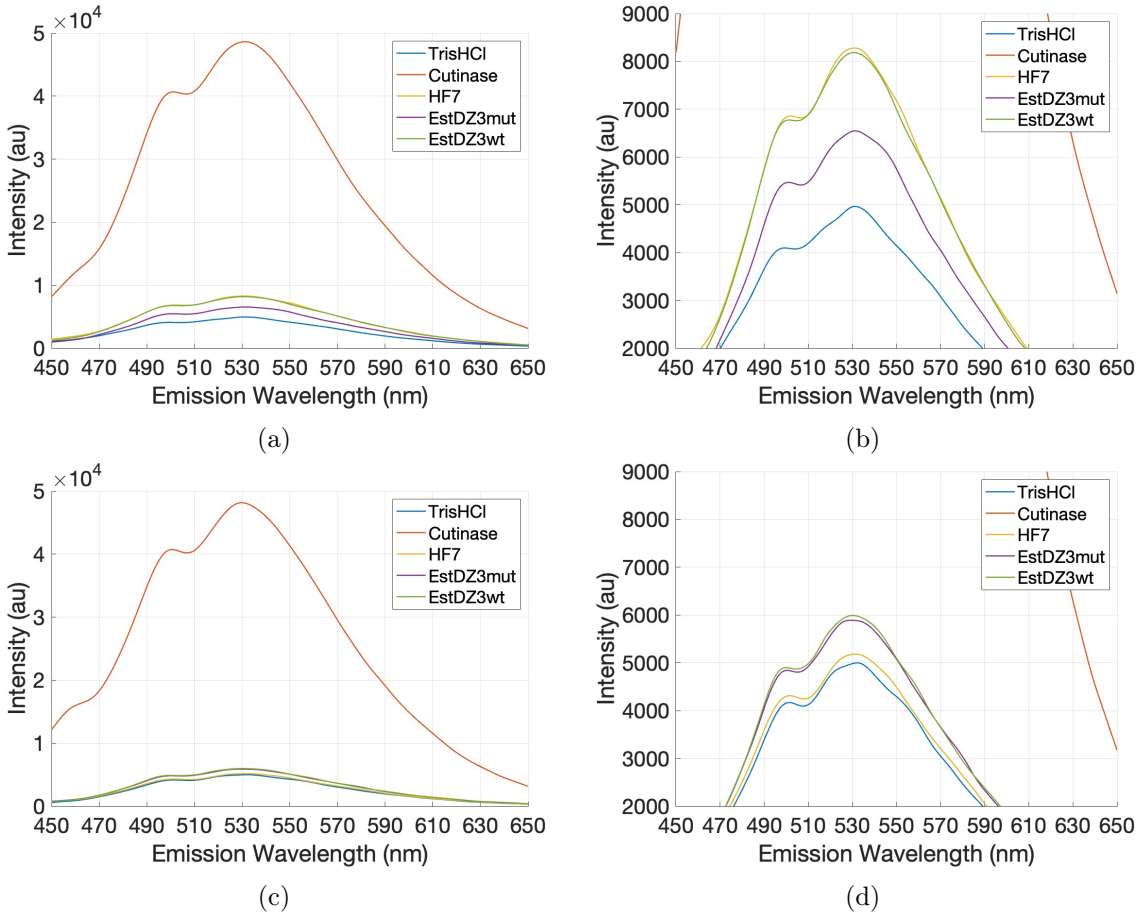

Figure 4.14: Emission spectra of the IA samples, respective to 410 nm excitation. (a,b) samples from Set I - only centrifuged after incubation. y-axis adjusted in (b) for comparison. (c,d) samples from Set II - centrifuged both prior to protein exposition and post incubation. y-axis adjusted in (d) for comparison.

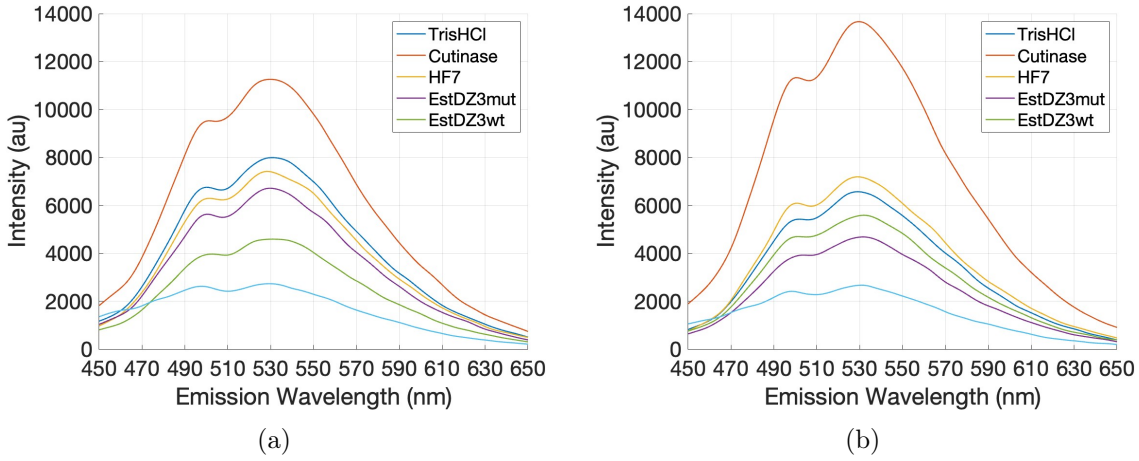

Figure 4.15: Emission spectra of the DA samples, respective to 410 nm excitation. (a) Set I, centrifuged after incubation. (b) Set II, centrifuged both prior to protein exposition and post incubation.

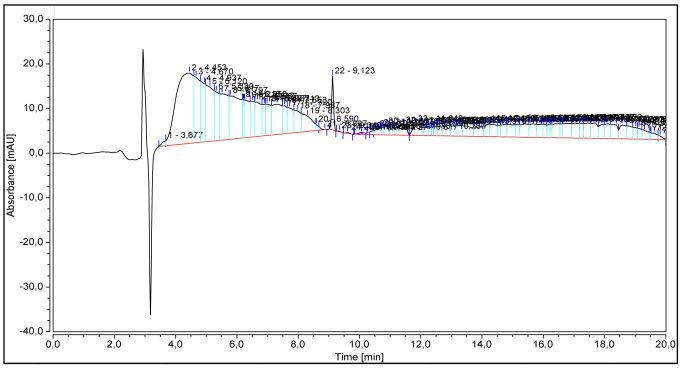

(a)

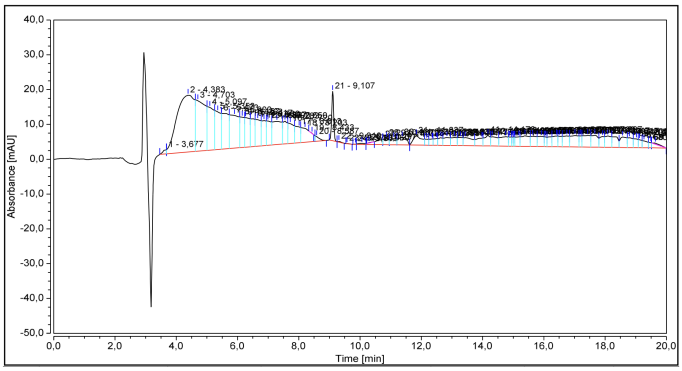

(b)

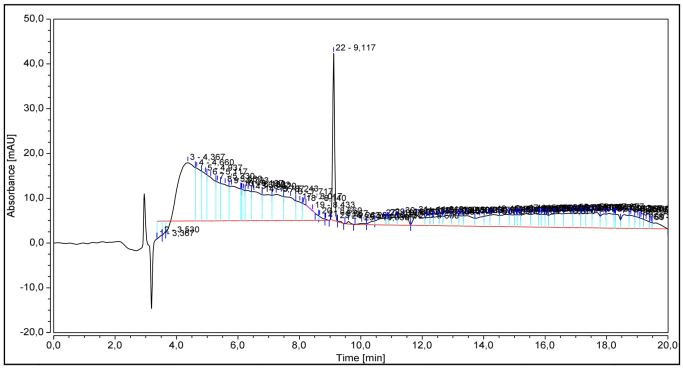

(c)

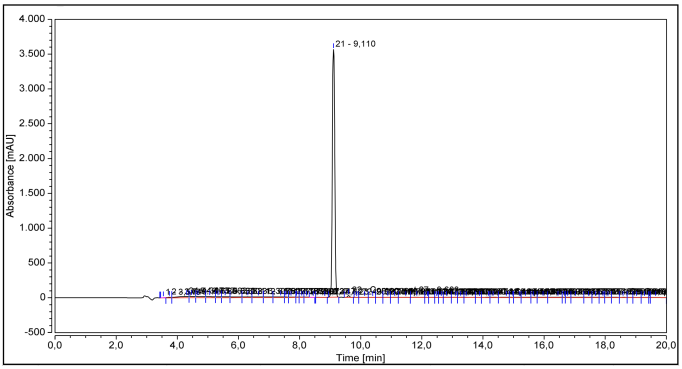

(d)

Figure 4.16: HPLC chromatograms obtained from the Department of Chemistry and BioScience, depicting 241 nm absorption with respect to retention time. Absorption peaks are annotated together with their retention times, peaks at 9 minutes correspond to TPA retention time. (a) sample incubated with HSH-25 (DA, Set I); (b) sample incubated with HSH-25 (DA, Set II); (c) sample incubated with cutinase (DA, Set I); (d) sample incubated with cutinase (IA, Set I).

Conclusion 5

Three types of CD (CD1, CD2, and CD3) were successfully synthesized and characterized according to size and fluorescent properties. Among them, CD2 was selected for further experimentation due to its fluorescent properties allowing for easier detection. The CD was then successfully integrated into PET substrates. Initial characterisations of spincoated CD-enriched PET films revealed the substrate to show loss of fluorescence for temperatures above 30 °C, limiting its applications fot enzyme screening. This issue led to the fabrication of electrospun CD-enriched PET fibers instead, which showed consistent fluorescence up to 60 °C while also providing a higher surface area available for protein interaction. Catalytic activity assays were initially performed using cutinase from *Fusarium solani* and peptide HF7, showing successful degradation of the PET substrate, with significant release of CD resulting from cutinase activity. Fiber removal from the substrate was confirmed by SEM imagining for both proteins, yet the lower intensity of fluorescence emission resulting from the peptide degradation underlined the need for optimizing the assay conditions in order to increase sensitivity. Three subsequent catalytic activity assays were performed, each with adjustments to the experiment conditions and to substrate fabrication. Additionally, the assays were progressively extended to include more proteins, notably peptide HSH-25, Esterase DZ3 and Esterase DZ3 mutant I144F M203Y.

Overall, the catalytic activity assays conducted on CD-enriched PET fibers validate the method as a proof-of-concept for using carbon dots as visual markers to report PET degradation. PET fibers incubated with cutinase consistently showed a significant increase in fluorescence emission associated with fiber removal, as measured by a combination of fluorescence spectrometry and HPLC measurements. However, the method failed to consistently report PET degradation for other catalysts tested. In separate instances, the presence of PET degradation product TPA was detected by HPLC for the peptide HSH-25 and Esterase DZ3 mutant I144F M203Y, without a corresponding increase in fluorescence emission. Furthermore, the formation of potential protein-CD complexes, and their resulting effect in fluorescence emission, requires further investigation before the method can be considered for high-throughput screening of PET-degrading enzymes. Nevertheless, these findings provide a novel approach for using carbons dots as visual indicators of PET degradation, which can serve as a basis for developing high-throughput enzyme activity assays. Future developments should focus on assessing the assay sensitivity, which could be achieved by using cutinase as positive control in a range of concentrations; exploring optimal ratios of CD to PET content in substrate fabrication and investigating potential fluorescence quenching from protein-CD interactions. Finally, if the method is optimized to reliably screen different catalysts, it could be adapted for use with other synthetic polymers, substantially contributing to advancements in biorecycling and the environmental sustainability of plastic waste management.

Bibliography

[1] C. Ostle, R. C. Thompson, D. Broughton, L. Gregory, M. Wootton, and D. G. Johns, "The rise in ocean plastics evidenced from a 60-year time series," eng, *Nature communications*, vol. 10, no. 1, pp. 1622–1622, 2019, ISSN: 2041-1723.

[2] Y. Chae and Y.-J. An, "Current research trends on plastic pollution and ecological impacts on the soil ecosystem: A review," *Environmental Pollution*, vol. 240, pp. 387–395, 2018, ISSN: 0269-7491. DOI: https://doi.org/10.1016/j.envpol.2018.05.008. Available: https://www.sciencedirect.com/science/article/pii/S0269749117348637.

[3] I. Ibrahim, A. G. Ashour, W. Zeiada, N. Salem, and M. Abdallah, "A systematic review on the technical performance and sustainability of 3d printing filaments using recycled plastic," *Sustainability*, vol. 16, no. 18, 2024, ISSN: 2071-1050. DOI: 10.3390/su16188247. Available: https://www.mdpi.com/2071-1050/16/18/8247.

[4] S. Al-Salem, P. Lettieri, and J. Baeyens, "Recycling and recovery routes of plastic solid waste (psw): A review," eng, *Waste management (Elmsford)*, vol. 29, no. 10, pp. 2625–2643, 2009, ISSN: 0956-053X.

[5] R. Koshti, L. Mehta, and N. Samarth, "Biological recycling of polyethylene terephthalate: A mini-review," eng, *Journal of polymers and the environment*, vol. 26, no. 8, pp. 3520–3529, 2018, ISSN: 1566-2543.

[6] T. Muringayil Joseph *et al.*, "Polyethylene terephthalate (pet) recycling: A review," *Case Studies in Chemical and Environmental Engineering*, vol. 9, p. 100 673, 2024, ISSN: 2666-0164. DOI: https://doi.org/10.1016/j.cscee.2024.100673. Available: https://www.sciencedirect.com/science/article/pii/S2666016424000677.

[7] C. I. Digest, "Carbios and de smet together to construct pet biorecycling plant," eng, *Chemical industry digest (Mumbai)*, 2024, ISSN: 0971-5266.

[8] "Carbios partners to commercialize enzyme-based pet recycling technology," *Focus on Catalysts*, vol. 2019, no. 8, pp. 6–7, 2019, ISSN: 1351-4180. DOI: https://doi.org/10.1016/j.focat.2019.07.041. Available: https://www.sciencedirect.com/science/article/pii/S1351418019303599.

[9] S. Sun, "Recent advances in screening and identification of pet-degrading enzymes," *Environmental Reviews*, vol. 32, no. 3, pp. 294–314, 2024. DOI: 10.1139/er-2023-0107. eprint: https://doi.org/10.1139/er-2023-0107. Available: https://doi.org/10.1139/er-2023-0107.

[10] C. J. Patel, R. H. Kansagara, D. V. Modi, N. J. Dudhat, K. H. Sojitra, and D. M. Babaria, "Microbes breaking down plastic: Insights for sustainable waste management," eng, *Nature environment and pollution technology*, vol. 23, no. 3, pp. 1717–1722, 2024, ISSN: 2395-3454.

[11] R. Wei, T. Oeser, S. Billig, and W. Zimmermann, "A high-throughput assay for enzymatic polyester hydrolysis activity by fluorimetric detection," eng, *Biotechnology journal*, vol. 7, no. 12, pp. 1517–1521, 2012, ISSN: 1860-6768.

[12] C. M. Carr, D. J. Clarke, and A. D. W. Dobson, "Microbial polyethylene terephthalate hydrolases: Current and future perspectives," *Frontiers in Microbiology*, vol. 11, 2020, ISSN: 1664-302X. DOI: 10.3389/fmicb.2020.571265. Available: https://www.frontiersin.org/journals/microbiology/articles/10.3389/fmicb.2020.571265.

[13] M. R. Belisário-Ferrari, R. Wei, T. Schneider, A. Honak, and W. Zimmermann, "Fast turbidimetric assay for analyzing the enzymatic hydrolysis of polyethylene terephthalate model substrates," eng, *Biotechnology journal*, vol. 14, no. 4, e1800272–n/a, 2019, ISSN: 1860-6768.

[14] T. B. Thomsen, S. W. Schubert, C. J. Hunt, P. Westh, and A. S. Meyer, "A new continuous assay for quantitative assessment of enzymatic degradation of poly(ethylene terephthalate) (pet)," eng, *Enzyme and microbial technology*, vol. 162, pp. 110 142–110 142, 2023, ISSN: 0141-0229.

[15] E. Ambrose-Dempster *et al.*, "Mechanoenzymatic reactions for the hydrolysis of pet," eng, *RSC advances*, vol. 13, no. 15, pp. 9954–9962, 2023, ISSN: 2046-2069.

[16] L. Đorđević, F. Arcudi, M. Cacioppo, and M. Prato, "A multifunctional chemical toolbox to engineer carbon dots for biomedical and energy applications," eng, *Nature nanotechnology*, vol. 17, no. 2, pp. 112–130, 2022, ISSN: 1748-3387.

[17] J. R. Lakowicz, *Principles of Fluorescence Spectroscopy*, eng, 3rd ed. Netherlands: Springer Nature, 2006, ISBN: 9780387463124.

[18] P. W. Atkins and R. S. Friedman, *Molecular Quantum Mechanics.* eng, 5. ed. Oxford: Oxford University Press, 2011, ISBN: 0199541426.

[19] D. Li and Y. Xia, "Electrospinning of nanofibers: Reinventing the wheel?" eng, *Advanced materials (Weinheim)*, vol. 16, no. 14, pp. 1151–1170, 2004, ISSN: 0935-9648.

[20] G. I. Taylor, "Electrically driven jets," eng, *Proceedings of the Royal Society of London. Series A, Mathematical and physical sciences*, vol. 313, no. 1515, pp. 453–475, 1969, ISSN: 1364-5021.

[21] D. H. Reneker and I. Chun, "Nanometre diameter fibres of polymer, produced by electrospinning," eng, *Nanotechnology*, vol. 7, no. 3, pp. 216–223, 1996, ISSN: 0957-4484.

[22] S. De Vrieze, T. Van Camp, A. Nelvig, B. Hagström, P. Westbroek, and K. De Clerck, "The effect of temperature and humidity on electrospinning," eng, *Journal of materials science*, vol. 44, no. 5, pp. 1357–1362, 2009, ISSN: 0022-2461.

[23] N. M. C. Mulkerns *et al.*, "Measuring the refractive index and sub-nanometre surface functionalisation of nanoparticles in suspension," *Nanoscale*, vol. 14, pp. 8145–8152, 22 2022. DOI: 10.1039/D2NR00120A. Available: http://dx.doi.org/10.1039/D2NR00120A.

[24] U. K. Laemmli, "Cleavage of structural proteins during the assembly of the head of bacteriophage t4," *Nature*, vol. 227, no. 5259, pp. 680–685, Aug. 1970, ISSN: 1476-4687. DOI: 10.1038/227680a0. Available: http://dx.doi.org/10.1038/227680a0.

[25] P. Kumar, S. Dua, R. Kaur, M. Kumar, and G. Bhatt, "A review on advancements in carbon quantum dots and their application in photovoltaics," *RSC Adv.*, vol. 12, pp. 4714–4759, 8 2022. DOI: 10.1039/D1RA08452F. Available: http://dx.doi.org/10.1039/D1RA08452F.

[26] X. Liu *et al.*, "Structure and photoluminescence evolution of nanodots during pyrolysis of citric acid: From molecular nanoclusters to carbogenic nanoparticles," *J. Mater. Chem. C*, vol. 5, pp. 10 302–10 312, 39 2017. DOI: 10.1039/C7TC03429F. Available: http://dx.doi.org/10.1039/C7TC03429F.

[27] A. Sharma and J. Das, "Small molecules derived carbon dots: Synthesis and applications in sensing, catalysis, imaging, and biomedicine," eng, *Journal of nanobiotechnology*, vol. 17, no. 1, pp. 92–92, 2019, ISSN: 1477-3155.

[28] S. Qu, X. Liu, X. Guo, M. Chu, L. Zhang, and D. Shen, "Amplified spontaneous green emission and lasing emission from carbon nanoparticles," eng, *Advanced functional materials*, vol. 24, no. 18, pp. 2689–2695, 2014, ISSN: 1616-301X.

[29] S. Qu *et al.*, "Toward efficient orange emissive carbon nanodots through conjugated sp2-domain controlling and surface charges engineering," eng, *Advanced materials (Weinheim)*, vol. 28, no. 18, pp. 3516–3521, 2016, ISSN: 0935-9648.

[30] N. Peng, K. Wang, N. Tu, Y. Liu, and Z. Li, "Fluorescence regional integration combined with parallel factor analysis to quantify fluorescencent spectra for dissolved organic matter released from manure biochars," *RSC Adv.*, vol. 10, pp. 31 502–31 510, 52 2020. DOI: 10.1039/D0RA02706E. Available: http://dx.doi.org/10.1039/D0RA02706E.

[31] B. Wang and S. Lu, "The light of carbon dots: From mechanism to applications," eng, *Matter*, vol. 5, no. 1, pp. 110–149, 2022, ISSN: 2590-2385.

[32] J. Li and X. Gong, "The emerging development of multicolor carbon dots," eng, *Small (Weinheim an der Bergstrasse, Germany)*, vol. 18, no. 51, e2205099–n/a, 2022, ISSN: 1613-6810.

[33] N. Javed and D. M. O'Carroll, "Long-term effects of impurities on the particle size and optical emission of carbon dots," *Nanoscale Adv.*, vol. 3, pp. 182–189, 1 2021. DOI: 10.1039/D0NA00479K. Available: http://dx.doi.org/10.1039/D0NA00479K.

[34] W. Bae, T.-Y. Yoon, and C. Jeong, "Direct evaluation of self-quenching behavior of fluorophores at high concentrations using an evanescent field," eng, *PloS one*, vol. 16, no. 2, e0247326–e0247326, 2021, ISSN: 1932-6203.

[35] A. Stockman and L. T. Sharpe, "Human cone spectral sensitivities and color vision deficiencies," eng, in *Visual Transduction and Non-Visual Light Perception*, ser. Ophthalmology Research, Totowa, NJ: Humana Press, pp. 307–327, ISBN: 9781588299574.

[36] J. Xue, T. Wu, Y. Dai, and Y. Xia, "Electrospinning and electrospun nanofibers: Methods, materials, and applications," *Chemical reviews.*, vol. 119, no. 8, 2019-04-24, ISSN: 0009-2665.

[37] L. H. Holst and F. T. Toftgård, "Design and exploration of small proteins that mimic natural protein functions," Supervised by Evamaria Petersen and Peter Fojan, M.S. thesis, Aalborg University, Aalborg, Denmark, Jun. 2023.

[38] S. U. Din *et al.*, "The purification and characterization of a cutinase-like enzyme with activity on polyethylene terephthalate (pet) from a newly isolated bacterium stenotrophomonas maltophilia prs8 at a mesophilic temperature," *Applied Sciences*, vol. 13, no. 6, 2023, ISSN: 2076-3417. DOI: 10.3390/app13063686. Available: https://www.mdpi.com/2076-3417/13/6/3686.

[39] A. K. Urbanek, K. E. Kosiorowska, and A. M. Mirończuk, "Current knowledge on polyethylene terephthalate degradation by genetically modified microorganisms," eng, *Frontiers in bioengineering and biotechnology*, vol. 9, pp. 771 133–771 133, 2021, ISSN: 2296-4185.

[40] V. Tournier *et al.*, "An engineered pet depolymerase to break down and recycle plastic bottles," eng, *Nature (London)*, vol. 580, no. 7802, pp. 216–219, 2020, ISSN: 0028-0836.

[41] K. Havlickova *et al.*, "The impacts of the sterilization method and the electrospinning conditions of nanofibrous biodegradable layers on their degradation and hemocompatibility behavior," *Polymers*, vol. 16, no. 8, 2024, ISSN: 2073-4360. DOI: 10.3390/polym16081029. Available: https://www.mdpi.com/2073-4360/16/8/1029.

[42] Y. Dong, S. Liao, M. Ngiam, C. K. Chan, and S. Ramakrishna, "Degradation behaviors of electrospun resorbable polyester nanofibers," *Tissue Engineering Part B: Reviews*, vol. 15, no. 3, pp. 333–351, 2009, PMID: 19459780. DOI: 10.1089/ten.teb.2008.0619. eprint: https://doi.org/10.1089/ten.teb.2008.0619. Available: https://doi.org/10.1089/ten.teb.2008.0619.

[43] M. T. Neves-Petersen, E. I. Petersen, P. Fojan, M. Noronha, R. G. Madsen, and S. B. Petersen, "Engineering the ph-optimum of a triglyceride lipase: From predictions based on electrostatic computations to experimental results," *Journal of Biotechnology*, vol. 87, no. 3, pp. 225–254, 2001, ISSN: 0168-1656. DOI: https://doi.org/10.1016/S0168-1656(01)00240-1. Available: https://www.sciencedirect.com/science/article/pii/S0168165601002401.

[44] Y. H. Hess, C. R. Bak, and J. Koch, "Design of a novel peptide with esterolytic activity towards pet by mimicking the catalytic motif of α/β-hydrolases," *Aalborg University Semester Project*, 2023.

[45] Y. H. Hess, C. R. Bak, and J. Koch, "Molecular modelling and *in silico* optimization of the thermophilic α/β-hydrolase estdz3," *Aalborg University Semester Project*, 2022.

[46] M. D. N. Micha Peleg and M. G. Corradini, "The arrhenius equation revisited," *Critical Reviews in Food Science and Nutrition*, vol. 52, no. 9, pp. 830–851, 2012, PMID: 22698273. DOI: 10.1080/10408398.2012.667460. eprint: https://doi.org/10.1080/10408398.2012.667460. Available: https://doi.org/10.1080/10408398.2012.667460.

[47] Y. Che *et al.*, "Microwave-assisted fabrication of copper-functionalized carbon quantum dots for sensitive detection of histidine," eng, *Talanta (Oxford)*, vol. 196, pp. 442–448, 2019, ISSN: 0039-9140.

[48] J. Liu, B. Song, and T. Fu, "Dual-emission fluorescence detection of histidine using carbon dots and calcein/ni2+ complexes," *Spectrochimica Acta Part A: Molecular and Biomolecular Spectroscopy*, vol. 286, p. 121 951, 2023, ISSN: 1386-1425. DOI: https://doi.org/10.1016/j.saa.2022.121951. Available: https://www.sciencedirect.com/science/article/pii/S138614252201099X.

[49] F. Zu *et al.*, "The quenching of the fluorescence of carbon dots: A review on mechanisms and applications," eng, *Mikrochimica acta (1966)*, vol. 184, no. 7, pp. 1899–1914, 2017, ISSN: 0026-3672.

[50] S. Bhattacharya, S. Nandi, and R. Jelinek, "Carbon-dot-hydrogel for enzyme-mediated bacterial detection," eng, *RSC advances*, vol. 7, no. 2, pp. 588–594, 2017, ISSN: 2046-2069.